A TECTONO-MAGMATIC CORRELATION OF BASALTIC ROCKS FROM OPHIOLITE MÉLANGES AT THE NORTH-EASTERN TIP OF THE SAVA-VARDAR SUTURE ZONE, NORTHERN CROATIA, CONSTRAINED BY GEOCHEMISTRY AND PETROLOGY

Damir Slovenec*,✉, Boško Lugović, Hans-Peter Meyer***** and **Gordana Garapić Šiftar°**

* *Croatian Geological Survey, Zagreb, Croatia.*

** *Institute of Mineralogy, Petrology and Mineral Deposits, Faculty of Mining, Geology, and Petroleum Engineering, University of Zagreb, Zagreb, Croatia.*

*** *Institute of Geosciences, University of Heidelberg, Germany.*

° *Department of Earth Sciences, Boston University, USA.*

✉ *Corresponding author, e.mail: dslovenec@hgi-cgs.hr*

Key-words: *Geochemistry, petrology, WPAB, E-MORB, T-MORB, N-MORB, IAT, ophiolite mélange, Sava-Vardar Suture Zone. Mts. Kalnik and Ivanščica, Croatia.*

ABSTRACT

Ophiolite mélanges of Mts. Kalnik and Ivanščica form the northern sector of the Kalnik Unit and represent the northeasternmost exposed tip of the Sava-Vardar Suture Zone. Petrological, geochemical and isotopic characteristics of extrusive rock blocks incorporated in the mélanges, particularly of pillow basalt altered to spilite, in association with radiolarian cherts, allow the rocks to be separated into five distinct groups. Each group has an age-marker based on the radiolarian assemblage in the associated cherts and/or on isotope dating which, along with previously published data on the Kalnik Unit, provide detailed analysis of the approximately 80 Ma long geodynamic evolution of the Repno Oceanic Domain - a part of the Meliata-Maliak ocean system. The rock groups are: (1) Late Anisian alkali basalts [$(La/Lu)_{cn}$ = 5.9-7.2; $\varepsilon_{Nd(T)}$ = +2.96; Cpx-TiO_2 = 3-6wt%] related to a terminal phase of intracontinental rifting; (2) enriched E-MORB-type basalts [$(La/Lu)_{cn}$ = 2.4-2.8; $\varepsilon_{Nd(T)}$ = +4.74; Cpx-TiO_2 = 2.1-2.9wt%] and depleted E-MORB-type basalts [$(La/Lu)_{cn}$ ~ 1.5; $\varepsilon_{Nd(T)}$ = +5.26; Cpx-TiO_2 = 1.9-2.3wt%] which reflect successive proto-oceanic crust formed at the ridge during the early Ladinian and late Ladinian, respectively; (3) middle Carnian T-MORB-type basalts [$(La/Sm)_{cn}$ = 0.79-0.87; $\varepsilon_{Nd(T)}$ = +6.63; Cpx-TiO_2 = 1.2-2.2wt%], representing crust from an evolved spreading center; (4) N-MORB-type basalts [$(La/Sm)_{cn}$ = 0.67-0.87; $\varepsilon_{Nd(T)}$ = +6.58; Cpx-TiO_2 = 0.6-1.9wt%] with inherited supra-subduction signature that diminish from the Late Carnian basalts [$(Nb/La)_n$ = 0.81] to the Bajocian basalts [$(Nb/La)_n$ = 1.1], and Middle Jurassic (Bathonian?) N-MORB-type basalts with recurrent subduction related influence [$(Nb/La)_n$ = 0.72; $(La/Sm)_{cn}$ = 0.76; $\varepsilon_{Nd(T)}$ = +6.23]; (5) late Bathonian medium-Ti [$(Nb/La)_n$ = 0.24-0.72; $\varepsilon_{Nd(T)}$ = +6.30; Cpx-TiO_2 = 0.6-1.1wt%] to late Oxfordian low-Ti IAT-type basalts [$(Nb/La)_n$ = 0.12-0.22; $\varepsilon_{Nd(T)}$ = +6.31; Cpx-TiO_2 = 0.2-0.6wt%] which reflect melts derived from a metasomatized and successively depleted mantle wedge in an extensional proto-arc setting.

INTRODUCTION

Ancient oceanic lithosphere may be preserved on land in large thrust sheets of relatively undisturbed and coherent lithostratigraphy (ophiolite complexes) thrust onto tectono-sedimentary units formed by a chaotic mixture of ophiolitic rock fragments, of various ages and lithology, embedded in a matrix during accretion, obduction and emplacement onto a continental margin (ophiolite mélange). Many authors maintain that ophiolites are mainly generated in suprasubduction settings, during intraoceanic subduction in the upper oceanic plate above the sinking slab (e.g., Shervais, 2001). Large and thick ophiolite thrust sheets record a geodynamic history from the formation of a metamorphic sole to the initiation of an island arc. Since this evolution lasts around 10 Ma (Stern, 2004) they record a relatively short history of oceanic crust generation. Thus, only the integrated study of ophiolite thrust sheets and the associated mélanges sheds light on the whole geodynamic evolution of an ancient oceanic domain, from intracontinental rifting, to onset of oceanization and ocean closure. Many integrated works suggest that the Neotethyan oceanic lithosphere was generated from (Early?) - Middle Triassic and continued to develop during Jurassic time (e.g., Smith et al., 1975; Robertson and Shallo, 2000; Robertson, 2002; Saccani et al., 2003; Bortolotti et al., 2004; Saccani et al., 2010).

In suture zones ophiolite mélanges contain fragments of mostly extrusive ophiolitic rocks of various sizes. Ophiolite mélanges are supposed to form in an accretionary wedge in front of a fore-arc, accordingly, they can receive magmatic material from both (oceanic) sides of the arc. Onset of subduction exposes progressively older oceanic crust to be scraped off from the subducting slab and consequently the mélange may incorporate older lithologies that were never found in the associated ophiolite, and which in turn are key rocks to trace the rest of the geodynamic history of an oceanic realm. In many mélanges, portions of extrusive rock sequences are the most abundant fragments. Among them, various types of pillow lavas best magmatic indicators of a geotectonic setting, associated with radiolarian cherts are particularly important because radiolarite associations provide the opportunity to date magmatic evolution inferred, in turn, from pillow basalt geochemistry. Excellent studies in this respect have been performed by Saccani and Photiades (2005) for the Albanide-Hellenide ophiolite mélanges; Gökten and Floyd (2007), Göncüoglu et al. (2010) for the ophiolite belt of the Izmir-Ankara-Erzincan suture zone and Vishnevskaya et al. (2009) for the Dinaride-Vardar ophiolite mélanges.

In the northeasternmost tip of the Sava-Vardar Suture Zone (SVSZ) four ophiolite sectors are split into the southern (Mts. Samoborska Gora and Medvednica) and northern

segment (Mts. Ivanščica and Kalnik) and are integrated into a single tectonostratigraphic unit, termed by Haas et al. (2000) - the Kalnik Unit. All sectors lack overthrust ophiolite. The Kalnik Unit recorded a trench history of Middle Jurassic-Hauterivian age (Babić et al., 2002). Studies on the southern mélange sectors (Slovenec and Lugović, 2008; 2009; Slovenec et al., 2010) provide good evidence for the initial and terminal stages of geodynamic evolution in the Repno Oceanic Domain (ROD) to which the Kalnik Unit belongs. The aim of this work was to extend research to the northern segment with the intention of identifying new extrusive lithologies which could help reconstruct the missing period of initial ocean spreading, via mature ocean stage, to the initiation of intraoceanic convergence. We studied the Nd and Sr isotopic compositions and the geochemical and petrological features of the extrusive blocks, in particular of a pillow basalt-radiolarian chert association from the mélange. Five different geochemical groups were recognised and were dated either by K-Ar, or, most frequently, indirectly by radiolarian assemblages in associated radiolarian cherts. Acquired results are supported by previously obtained data for the southern mélange segment and allow to reconstruct a liable geodynamic model for the entire ROD as a discrete domain of the Meliata-Maliak oceanic system.

GENERAL GEOLOGICAL FRAMEWORK

Mts. Kalnik and Ivanščica along with Mts. Medvednica and Samoborska Gora represent triangular intra-Pannonian innselbergs forming a junction between the Southeastern Alps, the Tisia continental block and the Internal Dinarides (Fig. 1A and 1B-C). These inselbergs are sheared between two regional fault zones, the Zagreb-Zemplin lineament in the south, and the Periadriatic-Balaton lineament in the north, and form the southwestern tip of the Zagorje-Mid-Trans-Danubian Zone (ZMTDZ; Fig. 1A) which extends about 100 km wide and 400 km long to the northeast (Pamić and Tomljenović, 1998). The inselbergs are located at the southwestern tip of ZMTDZ in the southern part of the Alpine-Carpathian-Pannonian (ALCAPA) block of the Intra-Carpathian Area (ICA) (Harangi et al., 1996) and consist of pre-Neogene heterogeneous, superimposed Dinaric and Alpine tectonostratigraphic and tectonometamorphic units of still debated origin (e.g., Pamić and Tomljenović, 1998; Tari and Pamić, 1998; Hass et al., 2000; Hass and Kovács, 2001; Pamić 2002). Structural and paleomagnetic data indicate that the pre-Neogene basement of the inselbergs experienced large regional-scale tectonic transport from NW and ca 130° CW rotation during Oligocene to early Miocene (Tomljenović et al., 2008) which resulted in their recent alignment almost perpendicular to the overall NW-SE Dinaric structural trend. Given its similar tectonostratigraphic evolution, Schmid et al. (2008) included the SW tip of the ZMTDZ in the SVSZ.

The Mts. Kalnik and Ivanščica ophiolite mélanges represent two separate northern sectors (Fig. 1B and 1C) and along with the southern sectors of Mts. Medvednica (Slovenec and Lugović, 2009) and Samoborska Gora (Slovenec et al., 2010) are assigned to a single tectonostratigraphic unit named the Kalnik Unit (Haas et al., 2000). This Unit can be interpreted as the remains of an oceanic segment termed the ROD by Babić et al. (2002). The ROD represents a cornerstone oceanic domain connecting the Vardar-Dinaridic ophiolites located to the SW and the Meliata-Maliak ophiolites to the NE. The accretion age of the Kalnik Unit based on matrix palynomorph assemblages is inferred to be Middle Jurassic to Hauterivian (Babić et al., 2002).

The surface geology of the Mts. Ivanščica and Kalnik is relatively simple and provides good tectono-stratigraphic constraints. The oldest rocks are Middle-Late Triassic limestones and dolomites from Mt. Ivanščica. They are intersected by a series of calc-alkaline extrusives and associated pyroclastic rocks which are interpreted as remnants of the late Anisian-Ladinian European continental margin volcanic arc (Goričan et al., 2005). The Middle-Late Triassic rock succession is in turn unconformably overlain by Late Jurassic to Early-Cretaceous limestones (Fig. 1C). This sedimentary succession of Mt. Ivanščica overthrust onto the ophiolite mélange or shows fault contacts. On the contrary, Mt. Kalnik completely lacks outcrops of Mesozoic carbonate rocks (Fig. 1B) but the mountain central ridge consists of Paleogene carbonate breccias which thrust over Neogene sedimentary rocks (Šimunić et al., 1981). Several tectonic slices of mantle peridotites were exhumed along the mountain ridge tectonic zone (Poljak, 1942). One of them is a few meters large composite slice, consisting of serpentinized lherzolite underlain by amphibolites (Lugović et al., 2007) which are interpreted as a metamorphic sole and dated on an amphibole separate to 118 Ma (Ignjatić, 2007). Both mélange sectors show either a tectonic-erosional unconformity against the youngest Neogene and Pleistocene sedimentary rocks or are faulty interfaced whilst the northern part of the Mt. Kalnik ophiolite mélange thrust onto the Neogene-Pleistocene sedimentary succession (Fig. 1B and 1C).

DESCRIPTION OF THE SAMPLED AREAS

The ophiolite mélanges of Mts. Kalnik and Ivanščica show similar structural features characterized by a block-in-matrix fabric, typical of chaotic complexes from subduction-related tectonic mélanges (Festa et al., 2010). They contain lithostratigraphically heterogeneous fragments of Mesozoic rocks ranging in size from pebbles and slivers to hectometer-kilometer large blocks embedded in a pervasively sheared continent-derived pelitic to siltitic matrix (Fig. 1B-C). Only two olistoliths from the Mt. Ivanščica mélange are composite - albeit without a boundary between the two rock types - all others in both mélanges are homogeneous. Sampling was particularly concentrated to coherent blocks composed of radiolarian cherts and extrusive rocks to analyse the chemical changes of extrusive rocks during ongoing oceanization of the ROD. The blocks which were already well dated through radiolarian assemblages but lacked geochemical data on the extrusive rocks were (re)analysed and presented in this work. Five geochemically different kinds of mafic extrusive rocks were recognized among the fragments: Group 1 (within plate alkali basalts = WPAB), Group 2 (enriched-mid-ocean ridge basalts = E-MORB), Group 3 (transitional-mid-ocean ridge basalts = T-MORB), Group 4 (very different varieties of essentially N-MORB-type (normal-mid-ocean ridge basalts), and Group 5 (island-arc tholeiites = IAT) as defined in the geochemistry section.

The Mt. Kalnik ophiolite mélange contains abundant clasts of ophiolitic rocks, mainly extrusives, (Vrkljan, 1989; Vrkljan and Vragović, 1991; Vrkljan, 1992; Pamić, 1997; Halamić, 1998; Vrkljan and Garašić, 2004), and subordinate fragments of sedimentary rocks (greywackes, minor shales,

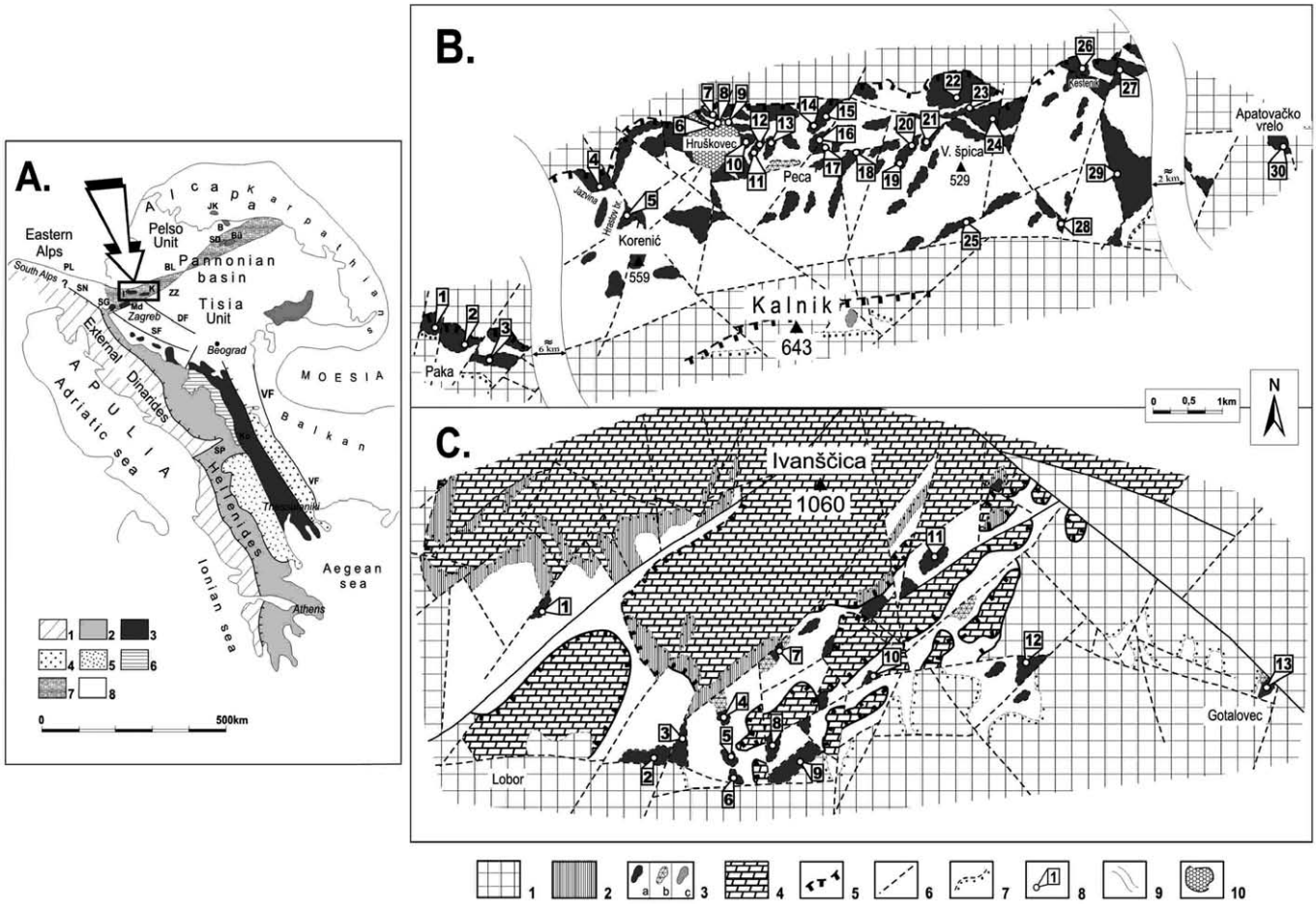

Fig. 1 - (A) Geotectonic sketch map of the Alps, Dinarides and Hellenides showing the position of the Sava-Vardar suture zone (after Pamić, 2000). Legend: 1- External units (External Dinarides and Alps); 2- Internal units [Passive continental margin, Central Dinaride Ophiolite Belt (CDOB), Mirdita Zone]; 3- Sava-Vardar Zone; 4- Serbo-Macedonian Massif; 5- Pelagonides; 6- Golija Zone; 7- Zagorje-Mid-Transdanubian Zone; 8- Panonian Basin. Faults: BL- Balaton; DF- Drava; PL- Periadriatic; SF- Sava; SP- Scutari-Peć; SN- Sava Nape; VF- Vardar; ZZ- Zagreb-Zemplin. Mountains: I- Ivanščica; K- Kalnik; Ko- Kopaonik; Md- Medvednica; SG- Samoborska Gora; SD- Szarvaskö-Darnó; Bü- Bükk. B- Bódva valley; JK- Jaklovce. Simplified geological map of: (B) Mt. Kalnik and (C) Mt. Ivanščica (modified after Šimunić et al., 1982 and Halamić, 1998). Legend: 1- Neogene and Pleistocene sedimentary rocks; 2- Jurassic-Cretaceous limestones; 3- ophiolite mélange with blocks of: 3a- basalt, 3b- gabbro, 3c- tectonite peridotite and Triassic-Jurassic radiolarites, sandstones and shales (not separated on the maps); 4- Triassic limestones and dolomites; 5- reverse or thrust faults; 6- normal faults; 7- discordance line, tectonic-erosion discordance; 8- sample location (Mt. Kalnik: 1 = vsk-215; 2 = vsk-214; 3 = vsk-211; 4 = ja-1, ja-2, ja-4; 5 = vsk-207, vsk-207a; 6 = vsk-24, h-23; 7 = h-5; 8 = h-26, h-27, vsk-240; 9 = h-33; 10 = vsk-221; 11 = vsk-222; 12 = vsk-223; 13 = vsk-224; 14 = vsk-234; 15 = vsk-238; 16 = vsk-235; 17 = vhk-236; 18 = vhk-23; 19 = vsk-18; 20 = vhk-15; 21 = vhk-11; 22 = vhk-47; 23 = vhk-6; 24 = kb-6, kb-7; 25 = vhk-463; 26 = ke-2, ke-15; 27 = vsk-210; 28 = ka-7; 29 = vsk-208; 30 = k-1; Mt. Ivanščica: 1 = vsi-13; 2 = pu-2; 3 = vsi-6/1, vsi-6/5, vsi-6/7; 4 = be-2; 5 = ib-2; 6 = ib-3; 7 = vsi-8/4; 8 = vsi-1; 9 = vsi-9; 10 = vsi-10; 11 = vsi-12; 12 = vsi-11; 13 = go-9, go-12, goi-2, got-6, gtc-1, gtc-2); 9- picture break; 10- quarry.

reddish and greyish cherts, scarce limestones) (Šimunić et al., 1982) along with minor blocks of non-ophiolitic extrusive rocks which have not been previously reported.

The oldest documented fragments in the Mt. Kalnik mélange are represented by the coherent olistolith of Group 1 pillow lavas at the top of massive lavas of the same group (Fig. 1B, location 21; NW from V. Špica). The latter ones show a K-Ar bulk rock Middle Triassic (Illirian, 235.8 Ma) age. These alkali extrusives were not found in the Mt. Ivanščica ophiolite mélange.

A slightly younger age, late Fassanian-early Langobardian, was determined by Goričan et al. (2005) for radiolarian cherts interbedded with massive basalt flows at Hrastov Brijeg (Fig 1B, location 5). Our analyses reveal Group 2 (E-MORB-type) geochemical signatures for these massive basalts. Similar E-MORB-type compositions are also found in the lower level of the Hruškovec quarry (Fig. 1B, location 6). However, some blocks of these E-MORB-type extrusive rocks consist of peperites and peperitic hyaloclastites in a very altered sedimentary matrix (Palinkaš et al., 2008). An upper level of the quarry (Fig 1B, location 7) exposes a layer of approximately 2 m thick late Ladinian (Langobardian) radiolarian cherts on top of the pillow lava complex (Goričan et al., 2005) which shows depleted E-MORB-type characteristics.

About 4 km east of the Hruškovec quarry, at the Kestenik locality (Fig 1B, location 26) a hectometer-large block composed of radiolarian chert layers crops out between the underlying pillow lavas and overlying massive lavas. Chert radiolarian biostratigraphy revealed a middle-late Carnian age (Halamić and Goričan, 1995; Goričan et al., 2005); both types of the associated Group 3 lava flows have transitional E-MORB/N-MORB geochemical signatures (termed T-MORB-type).

In the abandoned quarry at the Jazvina Stream (Fig 1B, location 4), about 1.5 km WSW of the Hruškovec quarry, dark red cherts directly overlain by pillow lavas gave a latest Carnian-middle Norian radiolarian assemblage (Halamić and Goričan, 1995; Goričan et al., 2005). The associated Group 4 pillow lavas show compositions typical of N-MORB.

An Early Jurassic age (Pliensbachian and Aalenian, 196-179 Ma) was documented by bulk rock K-Ar data performed on MORB-type gabbros and dolerites from uncertain locations approximately 1 km south of the Hruškovec quarry (Pamić, 1997).

The sheared horizon from the lower level in the Hruškovec quarry, 3-4 m above location 6 (Fig. 1B) contains meter-sized olistoliths of radiolarian cherts juxtaposed to similar sized blocks of massive lava flows set in a siltitic matrix (Fig 1B, location 8). The cherts contain a Middle Jurassic (late Bajocian-Callovian) radiolarian fauna (Goričan et al., 2005). K-Ar measurements performed on a plagioclase separate from a Group 5 (medium-Ti basalt IAT) block from this horizon yielded a similar Jurassic age (Bathonian, 164.7 Ma).

The Mt. Ivanščica ophiolite mélange exclusively contains blocks of Group 4 (N-MORB-type) and Group 5 (IAT-type) compositions. Compared to its Mt. Kalnik counterpart, this mélange contains more plutonic lithologies (Golub and Vragović, 1960; Golub and Šiftar, 1965) and less radiolarian cherts (Fig. 1C). Fragments of extrusive rocks are never found in close association with cherts, making it difficult to determine the ages of the different basalts. One hectometer large block of low-Ti IAT-type pillow lava from an abandoned Gotalovec quarry (Fig 1C, location 13) yielded a Middle Jurassic (late Oxfordian, 154.7 Ma) bulk rock K-Ar age. Another block from the same location is composed of Group 5 medium-Ti and low-Ti basalts. The largest block from the Mt. Ivanščica ophiolite mélange situated at its SW tip (Fig. 1C, location 3) is also composite and contains extrusives of Group 4 and medium-Ti basaltic rocks of Group 5, respectively.

ANALYTICAL TECHNIQUES

Mineral chemistry analyses from 19 samples were performed at the Mineralogical Institute, University of Heidelberg, Germany, using a CAMECA SX51 electron microprobe equipped with five wavelength-dispersive spectrometers. Measurements were performed using accelerating voltage of 15 kV, beam current of 20 nA, beam size of ~ 1 μm (for feldspars 10 μm) and 10s counting time for all elements. Natural minerals, oxides and silicates were used for calibration. Raw data for all analyses were corrected for matrix effects with the PAP algorithm (Pouchou and Pichoir 1984; 1985) implemented by CAMECA.

Bulk-rock powders for chemical analyses of 57 samples were obtained from rock chips free of veins. Samples with calcite-filled amygdals were dissolved in diluted HCl. The samples were analysed by ICP for major elements, and ICP-MS for all trace elements, at Actlab Laboratories in Ancaster, Canada. International mafic rocks were used as standards. Major element and trace element concentrations were measured with accuracy better than 1% and 5%, respectively.

Isotopic analyses were done in CRPG in Vandoeuvre, France, on a Triton Plus mass spectrometer. Normalizing ratios of $^{86}Sr/^{88}Sr = 0.1194$ and $^{146}Nd/^{144}Nd = 0.7219$ were assumed. The $^{87}Sr/^{86}Sr$ ratio for the NBS 987 Sr standard for the period of measurement was 0.710242±0.000030 (2σ). The $^{143}Nd/^{144}Nd$ ratio for the La Jolla standard was 0.5118451±0.000010 (2σ). Total procedural blanks were ~ 500 pg and ~ 150 pg for Sr and Nd, respectively.

The K-Ar measurements were performed on two whole rock samples and one plagioclase separate. Plagioclase was separated by an electromagnetic separator and standard heavy liquid techniques and purified by hand picking. The K concentration and Ar isotope were determined by ICP and isotope dilution procedure on noble gas mass spectrometry, respectively. The analyses were performed at the Activation Laboratories in Ancaster (Canada), using the method described by Dalrymple and Lanphere (1969).

PETROGRAPHY AND MINERAL CHEMISTRY

Extrusive rocks from the Mts. Kalnik and Ivanščica ophiolite mélanges comprise pillow lavas and massive lavas of essentially five geochemical groups: alkali WPB, E-MORB, T-MORB, N-MORB and IAT, which are petrographically described as Group 1, 2, 3, 4 and 5, respectively. Despite severe polyphase alteration, igneous textures are preserved in all samples. Textural features and mineral compositions of different rocks groups may be apparently similar, but their differences are best reflected by clinopyroxene and spinel chemistry.

Alkali extrusives of Group 1 from the Mt. Kalnik ophiolite mélange are aphyric and show quenched textures typical of a high cooling rate at the time of effusion. The lavas are amygdaloidal with up to 30% calcite amygdals. Some rock domains are characterized by spinifex to variolitic microtextures formed by intergrown abundant sheaf- or plumose-textured dark pink clinopyroxene and acicular plagioclase with thin glass infillings. Accessory spinel (Mg# = 44.7-65.0, Cr# = 0.37-0.41; TiO_2 = 1.31-2.67wt%) is a primary phase in all these basalts, occasionally coexisting with Al- and Cr-rich Ti-magnetite (4.7wt% TiO_2, 2.2wt% Al_2O_3, 1.6wt% Cr_2O_3). Plagioclase is always altered to albite ($An_{0.9-2.5}$) and/or peristerite ($An_{6.6-8.8}$) and very seldom to Al-rich pumpellyite. Clinopyroxenes are fresh or slightly altered to clinochlore-penninitic chlorite. Interstitial glass is devitrified to an aggregate of chlorite, calcite, hematite, prehnite, pumpellyite and titanite.

Tholeiitic extrusives of Groups 2-4 from the Mts. Kalnik and Ivanščica ophiolite mélanges occur as pillow and massive lavas, the latter being more abundant. They show similar mineral paragenesis of plagioclase, clinopyroxene, spinel, Ti-magnetite (1.3-6.5wt% TiO_2, 0.13-1.1wt% Al_2O_3 for Groups 2 and 3) and accessory apatite. N-MORB-type basalt of Group 4, sample vhk-15 (Fig. 1B; location 20) is a mineralogical exception that includes olivine phenocrysts enclosing spinel pseudomorphosed by diabantitic chlorite. Pillow lavas are fine- to very fine-grained aphyric to slightly plagioclase-clinopyroxene-phyric with ophitic to intergranular groundmass and show an outer chilled zone with porphyric plumose-variolitic to intersertal hypocrystalline texture. Calcite and/or chlorite filled amygdaloidal pillow lavas are common. Massive lavas are mostly aphyric to clinopyroxene-glomerophyric and show fine- to medium-grained holocrystalline intergranular texture. Petrographical evidence in basalts of Group 4 suggests the following order of crystallization: ± (spinel → olivine →) plagioclase → plagioclase + clinopyroxene ± Ti-magnetite (4.5-8.8wt% TiO_2, 0.6-0.9wt% Al_2O_3).

Clinopyroxene is systematically changed from pink in Group 2 through light pink in Group 3 to light brown or colorless in Group 4, suggesting significant differences in the mineral chemistry (see below). The change in clinopyroxene chemistry is also systematically followed by change in composition of the related spinel. Spinels hosted in basalts of Group 2 (E-MORB-type) show narrow compositional variation in terms of Mg# and Cr# (72.0-74.8 and 0.31-0.35, respectively), whereas TiO_2 contents vary significantly from 0.37-0.47wt% to 0.28-0.32wt% in the depleted rocks of the group. Groundmass spinels in basalts from Group 3 (T-MORB-type) contain the highest TiO_2 of all tholeiitic rocks (1.28-1.47wt%) and display a more enriched composition compared to the spinel assemblage in the N-MORB-type basalts of Group 4 (Mg# = 55.7-57.5, Cr# = 0.42-0.43 vs Mg# = 71.7-73.0, Cr# = 0.27-0.29; TiO_2 = 0.34-0.44wt%). In Group 3 basalts plagioclase is completely altered to albite. Relic plagioclase in Group 2 reveals an overall measured composition range of $An_{44.2\text{-}37.7}$. Plagioclase from Group 4 may be either continuously normally zoned, with core to rim compositions ranging from $An_{73.2}$ to $An_{56.7,}$ either reverse zoned ($An_{28.2}$ to $An_{54.0}$). The former compositional range resembles an entire compositional span of measured plagioclases. The primary assemblage is mostly altered to a suite of secondary minerals (albite, sericite, calcite, prehnite, diabantite-brunsvigitic chlorite, epidote, leucoxene, analcime and high-Al pumpellyite) indicating hydrothermal alteration within the lower greenschist facies allowing the rocks to be classified as spilites.

Tholeiitic extrusives of Group 5 from Mts. Kalnik and Ivanščica ophiolite mélanges also comprise pillow and massive lavas and show similar mineral compositions as Group 2-4 but different crystallization order: ± spinel (Mg# = 68.7-70.3, Cr# = 0.29-0.30; TiO_2 = 0.36-0.41wt%) → clinopyroxene → plagioclase ± Ti-magnetite (~5wt% TiO_2, ~1wt% Al_2O_3). The rocks are aphyric to slightly clinopyroxene-phyric with holocrystalline intergranular groundmass. Colorless clinopyroxene is slightly altered to brunsvigite-diabantitic chlorite. Plagioclase shows normal zoning with core to rim compositions of $An_{73.8}$ and $An_{48.1}$ respectively, which cover all measured plagioclase compositions of this geochemical rock group.

Clinopyroxene chemistry

Selected clinopyroxene compositions are shown in Table 1 and plotted in the classification diagram of Fig. 2, as well as in the discrimination diagram Fig. 3.

Dark pink clinopyroxenes from Group 1 basalts are normally zoned and show Al-Fe-diopsidic composition ($Wo_{46.3\text{-}50.1}$ $En_{25.1\text{-}39.8}Fs_{12.4\text{-}50.1}$) similar to clinopyroxenes from analogous Mt. Medvednica alkali basalts (Fig. 2). High contents of other-than-quadrilateral components (TiO_2 = 2.94-5.98wt%; Al_2O_3 = 5.47-8.72wt%) indicates a non-orogenic alkali nature of the host rocks (Leterrier et al., 1982). They are characterized by high Ti/Al ratio (0.36-0.49) which is favored by a high cooling rate of crystallization, magma chemistry and a cotectic spinel phase (Tracy and Robinson, 1977). In the clinopyroxene geotectonic discrimination diagram they plot beyond the relevant encountered fields, close to the TiO_2 apex (Fig. 3A) while in the MnO-TiO_2-Na_2O discrimination diagram after Nisbet and Pearce (1977) they plot in the field of Within-plate alkali basalts (not shown).

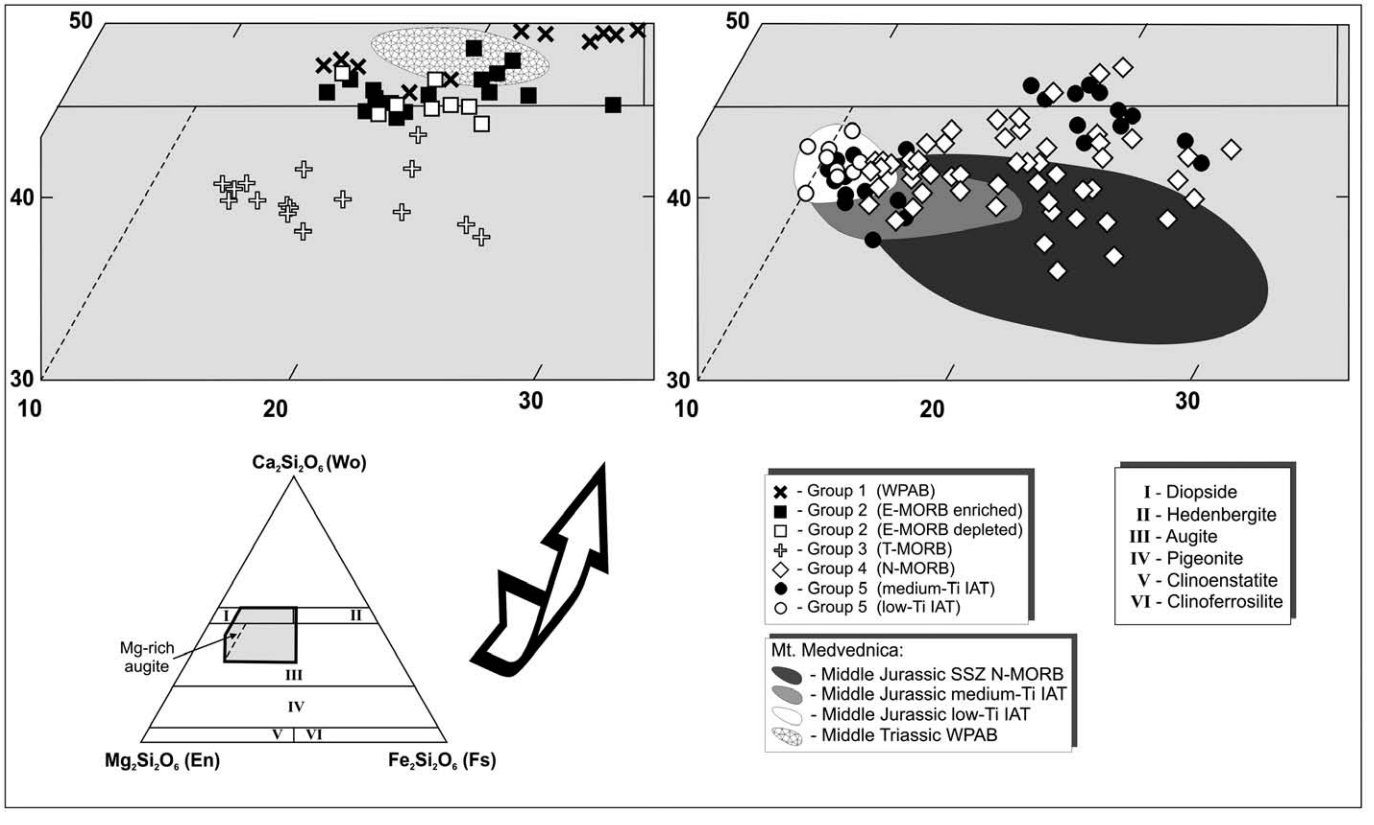

Fig. 2 - Plot of clinopyroxene compositions in the En-Wo-Fs ($Mg_2Si_2O_6$-$Ca_2Si_2O_6$-$Fe_2Si_2O_6$) diagram with the nomenclature fields of Morimoto (1988) for extrusive rocks from the Mts. Kalnik and Ivanščica ophiolite mélange. Fields of clinopyroxene compositions from basalts in the Mt. Medvednica ophiolite mélange (Slovenec and Lugović, 2009; Slovenec et al., 2010) plotted for correlation constraints.

Table 1 - Selected microprobe analyses and atoms per formula unit (a.p.f.u.) of clinopyroxene from the basaltic rocks in the Mts. Kalnik (KA) and Ivanščica (IV) ophiolite mélange.

	Group 1 – WPAB-type					Group 2 – E-MORB-type (enriched)				(depleted)			Group 3 – T-MORB-type					Group 4 – N-MORB-type		
Sample	kb-6	kb-6	*vhk-11	*vhk-11	*vhk-11	h-23	h-23	*vsk-207	*vsk-207	*h-33	*h-33	*h-33	*ke-15	*ke-15	vhk-47	vhk-47	vhk-47	vsk-215	vsk-215	vsk-221
Anal. nr.	1	15	1	2	19	5	6	16	18	1	12	15	16	22	2	18	19	34	35	3
Site	gm,c	gm,c	gm,c	gm,r	gm,c	gm,c	gm,r	gm,c	gm,c	gm,c	gm,c	gm,c	gm,r	gm,c	gm,r	gm,c	gm,r	gm,c	gm,r	gm,c
Rock type	PB	PB	MB	MB	MB	PB	PB	MB	MB	PB	PB	PB	PB	PB	MB	MB	MB	PB	PB	MB
Location	KA24		KA21			KA6		KA5		KA9			KA26		KA22			KA1		KA10
SiO_2	42.59	41.10	46.52	44.74	46.99	47.56	48.32	46.94	45.68	47.67	48.69	47.19	49.14	47.48	52.04	50.46	50.02	51.84	49.92	50.52
TiO_2	4.81	5.61	3.20	3.90	2.94	2.72	2.08	2.74	2.61	2.11	1.55	2.18	1.76	2.21	0.52	0.91	0.98	0.57	1.09	1.30
Al_2O_3	8.72	7.35	5.47	6.64	6.05	4.92	4.25	6.37	6.63	5.46	4.84	7.27	3.62	4.21	2.08	3.48	2.48	2.27	2.66	3.46
Cr_2O_3	0.09	0.06	0.03	0.00	0.20	0.18	0.11	0.36	0.25	0.35	0.15	0.23	0.28	0.20	0.28	0.18	0.00	0.18	0.06	0.21
FeO	10.79	13.76	9.42	10.30	7.17	9.83	9.44	9.94	12.11	10.79	9.75	7.69	10.99	11.46	7.77	9.07	13.41	6.86	12.82	7.76
MnO	0.17	0.23	0.28	0.17	0.17	0.21	0.21	0.25	0.23	0.19	0.22	0.19	0.30	0.25	0.18	0.23	0.47	0.20	0.40	0.22
MgO	9.77	7.93	12.44	11.43	13.22	12.63	12.88	11.97	10.54	11.81	12.85	12.81	13.26	11.66	16.94	15.70	13.24	16.56	14.66	15.07
CaO	22.08	22.01	21.48	21.14	22.06	20.79	20.93	20.92	20.58	20.83	21.11	21.62	19.63	20.58	19.82	18.79	18.52	20.62	16.99	20.63
Na_2O	0.49	0.59	0.46	0.48	0.37	0.51	0.47	0.39	0.47	0.48	0.36	0.38	0.40	0.50	0.27	0.29	0.28	0.23	0.29	0.33
Total	99.52	98.63	99.30	98.79	99.16	99.35	98.69	99.96	99.10	99.68	99.52	99.55	99.38	98.56	99.89	99.11	99.39	99.34	98.90	99.49
Si	1.624	1.607	1.756	1.706	1.761	1.793	1.830	1.764	1.746	1.798	1.829	1.761	1.855	1.818	1.913	1.881	1.898	1.916	1.890	1.877
Ti	0.138	0.165	0.091	0.112	0.083	0.077	0.059	0.077	0.075	0.060	0.044	0.061	0.050	0.064	0.014	0.026	0.028	0.016	0.031	0.036
Al^{IV}	0.376	0.338	0.243	0.294	0.239	0.207	0.170	0.236	0.254	0.202	0.171	0.239	0.145	0.182	0.087	0.119	0.102	0.084	0.110	0.123
Al^{VI}	0.016	0.001	0.001	0.005	0.028	0.012	0.019	0.046	0.044	0.041	0.043	0.081	0.016	0.007	0.003	0.034	0.009	0.015	0.008	0.029
Cr	0.003	0.002	0.001	0.000	0.006	0.005	0.003	0.011	0.008	0.010	0.004	0.007	0.008	0.006	0.008	0.005	0.000	0.005	0.002	0.006
Fe^{3+}	0.117	0.160	0.095	0.100	0.065	0.072	0.064	0.055	0.086	0.066	0.061	0.055	0.051	0.079	0.066	0.048	0.057	0.048	0.060	0.039
Fe^{2+}	0.227	0.290	0.203	0.228	0.159	0.238	0.235	0.257	0.301	0.275	0.245	0.185	0.296	0.288	0.173	0.234	0.368	0.165	0.346	0.202
Mn	0.005	0.008	0.009	0.005	0.005	0.007	0.007	0.008	0.007	0.006	0.007	0.006	0.010	0.008	0.006	0.007	0.015	0.006	0.013	0.007
Mg	0.555	0.462	0.700	0.650	0.739	0.710	0.727	0.671	0.601	0.664	0.720	0.713	0.746	0.665	0.929	0.873	0.749	0.912	0.827	0.835
Ca	0.902	0.922	0.869	0.864	0.886	0.840	0.849	0.842	0.843	0.842	0.850	0.865	0.794	0.884	0.781	0.751	0.753	0.817	0.689	0.821
Na	0.036	0.045	0.034	0.035	0.027	0.037	0.035	0.028	0.034	0.035	0.026	0.028	0.029	0.037	0.019	0.021	0.021	0.016	0.021	0.024
Total	4.000	3.999	4.000	4.000	4.000	4.000	4.000	3.996	3.999	3.999	4.000	4.000	4.000	4.000	3.999	4.000	4.000	4.000	4.000	4.000
Mg#	70.9	61.4	77.5	74.0	82.3	74.9	75.6	72.3	66.6	70.7	74.6	79.4	71.6	69.8	84.3	78.9	67.1	84.7	70.5	80.5
Al^{VI}/Al^{IV}	0.04	0.01	0.01	0.02	0.12	0.06	0.11	0.19	0.17	0.20	0.25	0.34	0.11	0.04	0.03	0.29	0.09	0.18	0.07	0.24

Table 1 (*continued*)

	Group 4 – N-MORB-type										Group 5 – IAT-type (medium-Ti)					(low-Ti)				
Sample	*ja-4	vhk-15	vhk-15	vhk-15	pu-2	pu-2	*vsi-6/5	ib-2	ib-2	ib-2	*h-26	*h-26	vsi-9	*vsi-6/1	*vsi-6/1	gtc-1	gtc-1	gtc-2	gtc-2	*got-6
Anal. nr.	5	34	35	37	6	7	11	5	18	19	20	27	23	25	26	1	2	6	8	10
Site	gm,c	gm,c	gm,r	gm,c	gm,c	gm,r	gm,c	gm,c	gm,c	gm,r	gm,c	gm,c	gm,c	gm,c	gm,r	gm,c	gm,r	gm,c	gm,c	gm,c
Rock type	MB	MB	MB	MB	MB	MB	PB	MB	MB	MB	MB	MB	MB	MB	MB	MB	MB	MB	MB	MB
Location	KA4	KA20			IV2		IV3	IV4			KA8		IV9	IV3		IV13		IV13		IV13
SiO_2	50.40	47.55	47.21	46.38	47.85	48.43	50.39	50.82	48.69	47.65	48.24	48.48	50.49	51.11	50.40	53.18	52.17	51.22	52.74	50.92
TiO_2	1.34	2.38	2.37	2.84	1.88	1.36	1.08	0.86	1.40	2.13	1.37	1.35	0.65	0.64	1.14	0.19	0.42	0.56	0.26	0.42
Al_2O_3	2.77	4.06	4.55	6.03	5.67	4.01	3.86	3.14	3.76	4.36	4.54	5.53	2.84	4.06	3.77	2.10	3.42	4.65	2.22	4.29
Cr_2O_3	0.00	0.01	0.06	0.25	0.28	0.11	0.29	0.20	0.03	0.03	0.15	0.23	0.08	0.52	0.22	0.14	0.30	0.51	0.38	1.10
FeO	10.50	14.36	13.61	10.43	8.87	12.18	8.24	7.85	11.4	14.02	11.21	9.78	8.16	5.90	7.12	5.92	6.05	5.99	4.44	5.18
MnO	0.25	0.29	0.31	0.16	0.20	0.27	0.15	0.30	0.30	0.36	0.20	0.25	0.33	0.20	0.16	0.22	0.18	0.10	0.24	0.14
MgO	13.84	10.61	11.27	11.14	13.37	13.54	16.06	15.95	14.11	12.33	11.76	12.29	17.17	16.84	15.76	18.33	16.88	16.73	17.83	16.01
CaO	20.06	19.68	19.71	21.49	20.94	18.18	19.51	20.34	18.97	18.12	20.71	21.35	18.34	19.59	20.71	19.78	20.29	20.02	21.67	21.66
Na_2O	0.42	0.58	0.52	0.45	0.38	0.35	0.25	0.35	0.36	0.39	0.44	0.39	0.24	0.32	0.26	0.17	0.24	0.26	0.22	0.22
Total	99.58	99.51	99.60	99.17	99.44	98.43	99.85	99.81	99.02	99.39	98.61	99.66	99.39	99.20	99.54	100.03	99.96	100.04	100.00	99.94
Si	1.891	1.821	1.800	1.764	1.791	1.844	1.860	1.875	1.836	1.815	1.840	1.820	1.905	1.882	1.864	1.936	1.908	1.870	1.918	1.866
Ti	0.038	0.069	0.068	0.081	0.053	0.039	0.030	0.024	0.040	0.061	0.039	0.038	0.018	0.018	0.032	0.005	0.012	0.015	0.007	0.012
Al^{IV}	0.109	0.179	0.200	0.236	0.209	0.156	0.140	0.125	0.164	0.185	0.160	0.180	0.095	0.125	0.136	0.064	0.092	0.130	0.082	0.134
Al^{VI}	0.014	0.004	0.004	0.034	0.041	0.024	0.028	0.012	0.003	0.011	0.044	0.065	0.029	0.058	0.028	0.026	0.056	0.070	0.013	0.051
Cr	0.000	0.000	0.002	0.008	0.008	0.003	0.008	0.006	0.001	0.001	0.005	0.007	0.002	0.015	0.006	0.004	0.009	0.015	0.011	0.032
Fe^{3+}	0.050	0.080	0.097	0.065	0.080	0.076	0.062	0.084	0.107	0.079	0.064	0.059	0.044	0.032	0.057	0.036	0.021	0.032	0.061	0.044
Fe^{2+}	0.280	0.380	0.337	0.267	0.197	0.312	0.193	0.159	0.253	0.368	0.294	0.248	0.208	0.149	0.163	0.144	0.164	0.151	0.074	0.115
Mn	0.008	0.009	0.010	0.005	0.006	0.009	0.005	0.009	0.011	0.012	0.006	0.008	0.010	0.006	0.005	0.007	0.006	0.003	0.007	0.004
Mg	0.774	0.606	0.640	0.632	0.746	0.769	0.884	0.878	0.793	0.700	0.669	0.688	0.945	0.925	0.869	0.994	0.921	0.911	0.967	0.874
Ca	0.806	0.809	0.804	0.876	0.840	0.742	0.772	0.804	0.767	0.740	0.846	0.859	0.726	0.773	0.821	0.771	0.795	0.784	0.844	0.850
Na	0.031	0.043	0.038	0.033	0.028	0.026	0.018	0.025	0.027	0.029	0.033	0.028	0.017	0.024	0.019	0.012	0.017	0.019	0.018	0.018
Total	4.000	4.000	4.000	4.000	4.000	4.000	3.999	4.000	3.999	4.000	4.000	4.000	4.000	3.999	4.000	4.000	4.000	3.999	3.999	3.999
Mg#	73.4	61.5	65.5	69.8	79.1	71.1	82.1	84.7	75.8	65.5	69.5	73.5	81.9	86.13	84.2	87.4	84.9	85.8	92.9	88.4
Al^{VI}/Al^{IV}	0.13	0.02	0.02	0.14	0.20	0.15	0.20	0.10	0.06	0.02	0.28	0.36	0.31	0.49	0.21	0.41	0.61	0.53	0.16	0.31

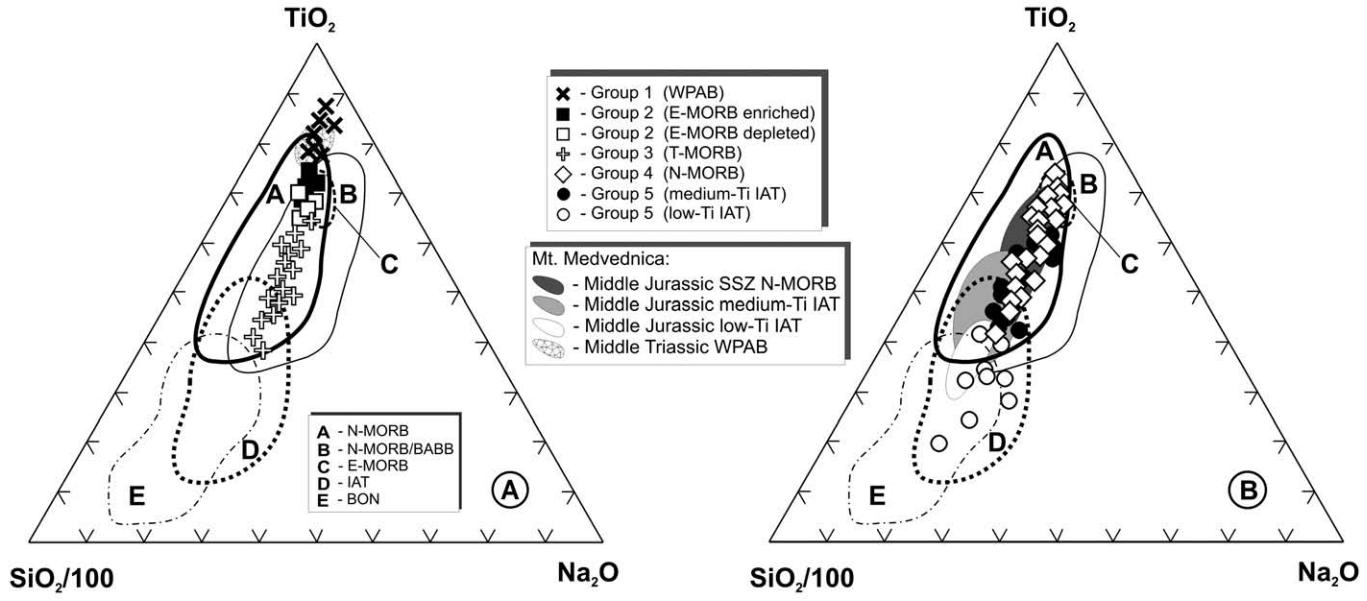

Fig. 3 - Discriminant diagram $SiO_2/100$ - Na_2O - TiO_2 (simplifed after Beccaluva et al., 1989) for clinopyroxene from the Mts. Kalnik and Ivanščica extrusive rocks: (A) Groups 1-3, (B) Groups 4-5. BABB- back-arc basalts; BON- boninite; IAT- island-arc tholeiites; E-MORB- enriched mid-ocean ridge basalts; N-MORB- normal mid-ocean ridge basalts. Fields of clinopyroxene compositions from basalts in the Mt. Medvednica ophiolite mélange (Slovenec and Lugović, 2009; Slovenec et al., 2010) plotted for correlation constraints.

Clinopyroxenes from the tholeiitic Groups 2-5 host rocks show normal discontinuous to oscillatory zoning with homogeneous core and decreasing Al^{VI}/Al^{IV}, Mg#, Cr and Ca and increasing Ti to the grain periphery (Table 1). Only clinopyroxene from Group 4 rocks may display reverse zoning. Significant compositional variations of phenocrystic versus matrix clinopyroxene of individual samples were not measured.

In Group 2 basalts clinopyroxenes from enriched varieties with composition $Wo_{45.0-48.8}En_{29.4-40.4}Fs_{13.2-25.1}$ lie in the field of diopside while clinopyroxenes from depleted varieties show composition $Wo_{44.2-47.4}En_{35.2.-39.1}Fs_{13.5-20.6}$ and lie on the boundary line between diopside and augite (Fig. 2). The clinopyroxenes from enriched and depleted basalts exhibit high TiO_2 contents (2.10-2.85wt% vs 1.89-2.32wt%) resulting in their high Ti/Al ratios (0.21-0.35 vs 0.19-0.28). The overall compositional characteristics of clinopyroxenes from this host rock group are similar to clinopyroxenes from E-MOR basalts (Beccaluva et al., 1989); in the clinopyroxene discrimination diagram for ophiolitic basalts they plot in the E-MORB field (Fig. 3A).

The clinopyroxenes from Group 3 rocks and some populations from Mt. Ivanščica Group 4 host basalts are augites ($Wo_{37.8-44.2}En_{35.0-47.5}Fs_{11.9-23.6}$ and $Wo_{35.6-44.9}En_{35.5-49.9}Fs_{11.1-24.4}$, respectively) and show a marked Fe-enrichment trend, very similar to clinopyroxenes from suprasubduction zone (SSZ) N-MORB from the Mt. Medvednica ophiolite mélange (Fig. 2). Clinopyroxene Mg# ranges from 65.5 to 84.7 without systematic differences between the groups. Compared to clinopyroxenes from the related Group 4 basalts from Mt. Ivanščica, those from Group 3 basalts have higher TiO_2 (1.22-2.21wt% vs 0.57-1.88wt%), but similar Ti/Al ratios (0.17-0.32 vs 0.11-31), suggesting a transitional chemistry of the latter group. The clinopyroxene population hosted in Group 4 basalts from the Mt. Kalnik ophiolite mélange forms a separate trend and resembles augite-diopside compositions ($Wo_{41.6-47.5}En_{32.2.-39.6}Fs_{16.5-42.9}$). These clinopyroxenes show the highest TiO_2 and Al_2O_3 contents (up to 2.84wt% and 6.52wt%, respectively) of all clinopyroxenes from Groups 3 and 4, suggesting that their host rocks may reflect different geotectonic settings. Despite their compositional diversity, all clinopyroxenes from Groups 3 and 4 basalts show geochemical signatures comparable to the N-MORB clinopyroxenes (Fig. 3 A-B).

Clinopyroxenes from Group 5 host basalts from Mt. Ivanščica are augites ($Wo_{37.5-45.0}En_{45.4-50.9}Fs_{7.3-15.6}$; Fig. 2) and form a compositional span concordant to the clinopyroxene hosted in the analogous rocks from the Mt. Medvednica ophiolite mélange described by Slovenec and Lugović (2009). The TiO_2 contents of clinopyroxenes hosted in the medium-Ti and low-Ti varieties may be significant (0.58-1.14wt% vs 0.19-0.56wt%) due to the fact that similar clinopyroxene Al_2O_3 contents result in Ti/Al ratios of 0.10-0.20 and 0.05-0.08, respectively. The Mg# of Ti-rich clinopyroxenes (82.0-89.7) is significantly lower than in the low-Ti clinopyroxene (83.8-92.8). In the discrimination diagram in Fig. 3B the Mt. Ivanščica clinopyroxene population of host rock Group 5 plots strictly in the field of IAT. The lowest Mg# (63.9-75.6) is estimated for the augite-diopside from Group 5 basalts in the Mt. Kalnik ophiolite mélange. Their core TiO_2 content averages 1.30wt% and their Ti/Al ratio is 0.16-0.32. They form a separate compositional trend at distinctly higher Wo- and Fs-contents ($Wo_{42.2-46.4}En_{33.8-38.6}Fs_{15.0-24.1}$; Fig. 2), which is similar to the trend of IAT medium-Ti basalts from the Mt. Samoborska Gora ophiolite mélange (Slovenec et al., 2010).

BULK ROCK CHEMISTRY

Chemical compositions of the analyzed rocks are shown in Table 2. Nd and Sr isotopic compositions of eight samples representative of all geochemical groups are displayed in Table 3.

Table 2 - Chemical analyses of basaltic rocks in the Mts. Kalnik (KA) and Ivanščica (IV) ophiolite mélange.

	Group 1 – WPAB-type							Group 2 – E-MORB-type (enriched)								(depleted)		Group 3 – T-MORB-type				
Sample	kb-6	kb-7	*vhk-11	vsk-210	vsk-211	vsk-234	vsk-238	h-23	*vsk-207	*vsk-207a	vsk-214	vsk-222	vsk-223	vsk-235	vsk-240	*h-33	*h-5	*ke-2	*ke-15	vhk-47	vsk-236	k-1
Rock type	PB	PB	MB	MB	MB	MB	MB	PB	MB	MB	MB	MB	MB	MB	PB	PB	PB	PB	MB	MB	MB	MB
Location	KA24	KA24	KA21	KA27	KA3	KA14	KA15	KA6	KA5	KA5	KA2	KA11	KA12	KA16	KA8	KA9	KA7	KA26	KA26	KA22	KA17	KA30
SiO_2	47.05	50.48	45.82	50.90	48.33	50.99	47.29	46.47	50.87	50.81	50.33	52.14	46.75	51.36	45.63	50.10	49.16	50.18	49.94	50.20	51.44	50.32
TiO_2	2.34	2.34	1.58	2.01	1.98	2.42	1.84	1.76	1.41	1.78	2.22	1.96	1.70	2.25	2.37	1.03	0.99	1.93	1.88	2.09	2.27	1.98
Al_2O_3	16.70	16.31	16.01	15.84	16.53	17.86	16.48	15.24	19.90	15.95	14.39	16.35	16.05	13.48	16.45	17.01	16.65	16.04	16.20	14.46	16.59	15.17
Fe_2O_{3total}	7.75	8.09	8.38	7.55	9.48	9.33	9.48	8.98	7.72	8.98	8.66	8.16	9.47	10.94	11.74	7.14	8.09	8.16	7.58	10.33	8.50	9.21
MnO	0.20	0.15	0.25	0.14	0.14	0.18	0.16	0.14	0.11	0.15	0.14	0.43	0.12	0.18	1.41	0.14	0.18	0.26	0.27	0.17	0.09	0.18
MgO	8.91	6.55	13.41	6.25	5.54	3.77	7.31	7.57	6.44	6.54	6.04	6.27	7.95	6.22	7.74	7.23	8.97	7.16	7.10	6.94	6.65	6.70
CaO	7.03	6.38	4.57	7.51	7.00	2.80	8.75	9.46	7.23	4.38	8.29	3.94	9.27	7.00	3.42	7.73	7.86	6.32	6.48	7.92	3.86	10.09
Na_2O	3.80	4.01	3.71	4.91	4.14	5.40	4.29	4.07	4.38	5.52	4.01	5.61	2.67	5.12	4.66	4.12	3.89	4.76	4.54	3.88	6.59	2.94
K_2O	0.31	1.14	0.46	0.23	1.02	1.89	0.20	0.53	0.65	0.72	0.67	0.63	0.58	0.69	0.59	0.57	0.28	0.62	0.74	0.75	0.73	0.78
P_2O_5	0.43	0.52	0.34	0.43	0.48	0.58	0.30	0.21	0.19	0.23	0.30	0.26	0.20	0.30	0.23	0.12	0.13	0.19	0.18	0.20	0.21	0.18
LOI	5.05	4.38	6.21	3.75	3.97	5.12	4.77	5.84	4.97	4.79	3.72	3.91	3.64	2.48	4.81	3.65	4.05	4.51	4.56	3.45	2.65	3.16
Total	99.57	100.40	100.70	99.51	98.61	100.30	100.90	100.30	101.90	99.85	98.77	99.66	99.03	100.00	99.05	98.84	100.30	100.10	99.48	100.40	99.58	100.70
Mg#	72.6	62.5	77.3	65.0	55.2	45.7	62.0	62.8	65.7	59.3	60.6	61.5	63.9	55.2	57.9	62.8	69.5	64.6	67.8	57.9	62.9	59.9
Cs	1.1	3.8	2.6	0.4	0.8	5.6	0.3	0.5	1.5	0.9	0.3	0.4	0.3	0.2	0.3	0.7	1.1	0.8	1.4	1.0	1.5	2.3
Rb	9	18	5	3	14	32	4	5	17	6	6	5	6	8	6	9	5	9	9	11	12	13
Ba	155	197	148	42	146	300	51	134	141	142	113	103	89	172	102	63	51	76	86	98	62	102
Th	3.22	3.17	2.53	3.29	2.98	3.75	2.93	0.91	0.86	1.05	1.39	1.26	1.25	1.35	1.41	0.37	0.33	0.49	0.45	0.55	0.57	0.51
Ta	2.60	2.56	1.94	2.54	2.31	2.76	2.18	0.61	0.57	0.67	0.84	0.74	0.63	0.91	0.93	0.23	0.22	0.23	0.30	0.34	0.36	0.33
Nb	42.0	39.6	31.3	39.4	36.0	44.0	34.0	10.3	9.5	11.3	14.6	12.7	10.6	15.6	15.8	3.8	3.6	5.2	4.9	5.5	5.7	5.3
Sr	347	351	233	149	364	403	130	244	297	233	379	321	233	225	365	230	219	238	290	298	301	287
Zr	187	171	128	182	163	234	154	109	98	113	149	122	104	152	156	73	70	138	135	149	154	143
Hf	4.4	4.1	3.0	3.9	4.0	5.4	3.5	3.1	2.9	3.4	4.3	3.9	3.0	4.6	4.7	1.9	1.8	3.5	3.4	3.7	4.1	3.6
Y	31.5	30.1	21.9	28.4	26.4	37.5	29.4	27.7	25.5	29.9	39.7	33.1	26.5	39.2	45.1	21.5	19.8	37.7	35.9	41.6	43.9	39.1
Sc	33	32	24	28	32	40	33	32	35	38	48	46	41	39	51	34	34	42	43	36	27	41
V	297	289	211	262	281	258	278	256	221	244	358	324	316	283	379	186	197	288	301	334	361	355
Cr	280	260	380	240	200	200	350	327	350	360	356	348	282	312	260	310	310	440	440	385	380	401
Ni	210	200	260	120	140	120	160	180	100	141	80	91	100	60	60	170	170	250	220	182	159	181
La	24.81	25.01	18.91	24.10	24.63	34.20	24.82	8.89	7.89	9.41	12.08	10.76	8.41	13.32	14.29	4.12	3.99	5.83	5.71	6.35	6.72	6.04
Ce	51.80	52.40	39.2	49.61	48.42	72.32	48.56	22.10	18.65	23.13	28.70	26.20	20.92	30.61	33.92	10.52	10.21	16.73	16.41	18.82	18.99	17.00
Pr	6.04	5.94	4.45	5.54	5.41	8.04	5.51	3.02	2.52	3.05	3.79	3.41	2.87	4.17	4.60	1.50	1.46	2.59	2.53	2.81	2.98	2.59
Nd	24.9	24.81	18.01	22.40	22.40	31.56	22.46	14.41	11.60	14.38	18.41	15.77	13.53	19.00	21.20	7.63	7.48	13.70	13.60	15.50	15.93	13.99
Sm	5.76	5.67	4.17	5.04	4.92	7.48	4.86	4.18	3.37	4.18	5.19	4.69	3.84	5.41	5.92	2.42	2.38	4.45	4.36	4.79	5.35	4.38
Eu	1.840	1.801	1.330	1.531	1.600	2.079	1.651	1.377	1.220	1.381	1.860	1.649	1.298	1.770	2.031	0.955	0.936	1.601	1.569	1.709	1.821	1.660
Gd	5.96	5.78	4.22	5.21	5.16	7.07	5.28	4.63	4.12	4.69	6.24	5.36	4.57	6.35	7.11	3.06	2.96	5.19	5.09	6.11	6.69	5.56
Tb	1.02	1.01	0.71	0.87	0.87	1.17	0.95	0.84	0.73	0.86	1.09	1.01	0.84	1.14	1.29	0.55	0.53	1.01	0.97	1.15	1.22	1.08
Dy	5.94	5.81	4.25	4.98	5.13	7.07	5.44	5.24	4.22	5.44	7.01	6.32	5.26	7.42	8.03	3.53	3.36	6.48	6.32	7.08	7.68	6.73
Ho	1.20	1.16	0.84	1.06	1.02	1.34	1.13	1.06	0.89	1.11	1.44	1.31	1.06	1.56	1.73	0.75	0.73	1.36	1.32	1.54	1.66	1.47
Er	3.35	3.22	2.37	2.92	2.86	3.71	3.13	3.00	2.48	3.11	4.02	3.74	2.87	4.21	4.69	2.18	2.07	3.89	3.81	4.44	4.78	4.14
Tm	0.501	0.481	0.355	0.428	0.442	0.561	0.482	0.433	0.361	0.442	0.581	0.530	0.425	0.607	0.691	0.331	0.315	0.611	0.581	0.676	0.727	0.652
Yb	3.10	3.01	2.21	2.79	2.69	3.66	2.90	2.74	2.30	2.91	3.59	3.38	2.66	3.78	4.41	2.01	1.95	3.63	3.63	4.40	4.57	3.93
Lu	0.447	0.439	0.324	0.397	0.384	0.511	0.414	0.393	0.327	0.422	0.531	0.488	0.384	0.545	0.619	0.297	0.282	0.523	0.515	0.637	0.679	0.571

Major elements are in wt %, trace elements in ppm. LOI = loss on ignition at 1100 °C. Legend: WPAB = within plate alkali basalt, E-MORB = enriched mid-ocean ridge basalt, T-MORB = transitional mid-ocean ridge basalt, N-MORB = normal mid-ocean ridge basalt; IAT = island-arc tholeiites; PB = pillow basalt, MB = massive basalt. *Age-marker of a rock group: Late Anisian WPAB-type, Early Ladinian enriched E-MORB-type, Late Ladinian depleted E-MORB-type, Middle Carnian T-MORB-type, Late Carnian N-MORB-type, Late Bathonian medium-Ti IAT-type, Late Oxfordian low-Ti IAT-type. Mg# = 100 * molar ($MgO/(MgO+FeO_{total})$)

Table 2 (*continued*)

	Group 4 – N-MORB-type																			Group 5 – IAT-type		
Sample	*ja-1	*ja-2	*ja-4	ka-7	vhk-6	vhk-463	vsk-208	vsk-215	vsk-221	vsk-224	vhk-15	*vsi-6/7	pu-2	*vsi-6/5	vsi-1	vsi-10	vsi-13	ib-3	ib-2	be-2	*h-26	h-27	vhk-23
Rock type	MB	MB	PB	MB	PB	MB	PB	PB	MB	MB	MB	PB	MB	PB	MB	MB	MB	MB	MB	MB	MB	PB	MB
Location	KA4	KA4	KA4	KA28	KA23	KA25	KA29	KA1	KA10	KA13	KA20	IV3	IV2	IV3	IV8	IV10	IV1	IV6	IV5	IV4	KA8	KA8	KA18
SiO_2	51.50	47.05	52.41	52.07	49.04	51.19	47.01	50.30	47.32	49.56	46.21	47.97	50.66	48.88	48.96	50.32	51.44	49.96	52.38	50.90	46.01	50.97	46.02
TiO_2	1.13	1.23	0.93	0.88	1.44	1.42	1.48	1.29	1.32	1.41	1.31	1.41	1.43	1.52	1.55	1.63	1.68	1.72	1.78	1.90	1.01	1.06	1.09
Al_2O_3	14.31	15.74	15.19	19.05	14.27	14.79	16.97	14.80	15.73	16.25	17.50	14.25	13.58	14.26	14.18	14.06	13.58	13.67	13.53	14.84	16.44	17.01	17.02
Fe_2O_{3total}	10.84	10.80	10.20	9.98	10.91	10.83	9.80	9.10	9.95	8.12	8.87	10.84	9.46	10.85	10.96	10.62	10.39	10.82	11.44	12.16	9.64	9.68	8.29
MnO	0.35	0.23	0.22	0.14	0.18	0.31	0.44	0.16	0.20	0.14	0.14	0.14	0.15	0.20	0.21	0.23	0.22	0.25	0.20	0.24	0.44	0.28	0.14
MgO	7.80	8.79	6.80	6.65	7.71	7.87	9.13	7.40	8.12	6.55	7.61	6.62	7.15	8.18	7.75	7.21	6.56	6.48	5.98	5.71	10.81	5.83	9.36
CaO	4.13	3.78	5.90	0.37	7.92	2.77	2.05	10.15	10.11	10.75	11.42	10.85	9.00	8.32	8.21	7.39	6.72	6.55	7.01	4.17	9.26	4.15	10.83
Na_2O	4.74	4.16	4.03	6.62	3.90	4.73	4.65	2.80	2.71	3.13	2.40	3.74	4.29	3.83	3.72	3.93	4.21	4.97	5.06	5.44	2.09	3.79	2.23
K_2O	0.33	1.40	0.54	0.13	0.74	0.52	0.73	0.48	0.34	0.65	0.07	0.10	0.13	0.37	0.11	0.09	0.09	0.08	0.02	0.13	0.11	0.18	0.11
P_2O_5	0.12	0.14	0.10	0.09	0.15	0.15	0.16	0.13	0.14	0.15	0.14	0.13	0.14	0.16	0.16	0.17	0.17	0.17	0.21	0.19	0.09	0.12	0.09
LOI	4.21	5.07	3.36	4.43	2.96	4.45	6.62	2.78	3.59	2.99	3.61	3.62	4.11	3.50	3.99	4.08	4.23	4.99	3.10	3.90	5.05	6.42	4.83
Total	99.46	98.39	99.68	99.53	99.22	99.03	99.04	99.39	99.53	99.70	99.28	99.67	100.10	100.07	99.80	99.73	99.29	99.66	100.71	99.58	100.90	99.49	100.00
Mg#	60.7	63.5	57.4	59.7	60.4	60.9	67.0	62.2	64.4	62.5	65.9	56.7	61.4	61.8	58.0	56.2	53.9	56.2	51.6	50.4	70.7	56.5	70.4
Cs	0.4	3.5	1.2	0.9	3.4	2.8	0.5	5.2	0.8	3.6	0.1	0.1	0.1	0.5	0.4	0.5	0.3	0.3	0.4	0.5	0.4	0.8	0.1
Rb	1	10	7	2	11	10	9	8	7	9	2	1	3	8	4	7	6	1	3	4	1	3	1
Ba	80	128	134	31	123	108	63	90	94	108	40	26	36	218	221	172	186	167	220	221	17	37	15
Th	0.14	0.26	0.16	0.15	0.28	0.27	0.32	0.21	0.27	0.27	0.29	0.28	0.32	0.31	0.33	0.39	0.46	0.54	0.64	0.58	0.18	0.34	0.20
Ta	0.01	0.16	0.11	0.09	0.17	0.17	0.19	0.15	0.15	0.17	0.16	0.16	0.15	0.19	0.18	0.18	0.19	0.18	0.20	0.20	0.03	0.08	0.04
Nb	0.2	2.7	1.7	1.4	2.8	2.8	3.1	2.5	2.6	2.8	2.6	2.7	2.4	3.0	2.8	2.9	3.0	2.9	3.2	3.2	0.5	1.2	0.6
Sr	105	89	103	83	143	155	153	149	139	154	92	78	123	105	112	165	148	188	115	183	108	163	165
Zr	38	87	55	51	95	94	98	79	85	93	94	93	92	105	113	121	128	133	146	138	61	70	78
Hf	1.2	2.6	1.7	1.5	2.8	2.8	2.9	2.4	2.5	2.7	2.7	2.6	2.6	2.9	3.0	3.2	3.3	3.4	3.7	3.7	1.7	2.0	2.1
Y	18.0	29	23	21	32	31	32	27	30	29	32	31	31	33	35	36	39	42	44	47	25	25	24
Sc	35	45	39	24	40	33	37	44	43	45	43	42	42	45	38	39	42	37	36	37	40	46	40
V	273	301	247	237	320	318	278	329	313	312	311	316	300	309	316	321	329	331	319	343	266	269	266
Cr	273	310	300	320	260	272	240	312	240	340	205	189	209	320	210	171	169	160	140	130	348	370	353
Ni	49	112	120	112	70	81	90	84	140	160	61	60	60	73	63	68	54	59	49	56	370	220	390
La	3.05	3.43	2.35	1.92	3.56	3.52	3.97	3.33	3.39	3.49	3.61	4.01	3.58	4.11	4.22	4.62	4.99	5.19	6.08	5.61	1.88	2.18	2.64
Ce	9.03	10.49	7.24	5.82	11.01	10.98	12.11	9.84	10.31	10.88	10.53	11.32	10.50	11.80	12.21	13.46	14.95	15.20	17.30	16.40	6.54	7.39	8.68
Pr	1.45	1.74	1.13	0.95	1.83	1.81	1.95	1.53	1.61	1.77	1.65	1.75	1.63	1.84	1.92	2.24	2.35	2.44	2.65	2.60	1.14	1.28	1.44
Nd	4.48	9.00	5.79	4.92	9.60	9.57	10.30	8.05	8.68	9.56	9.28	9.95	9.21	10.30	11.08	12.23	12.96	13.20	14.10	14.40	6.47	6.96	7.76
Sm	2.60	3.17	2.04	1.76	3.35	3.31	3.61	2.78	3.04	3.29	3.18	3.32	3.14	3.41	3.55	3.72	3.96	4.06	4.39	4.61	2.52	2.55	2.60
Eu	0.867	1.131	0.753	0.683	1.090	1.129	1.261	1.050	1.089	1.151	1.218	1.342	1.213	1.300	1.369	1.422	1.470	1.482	1.541	1.610	0.992	0.995	1.031
Gd	3.67	4.11	2.96	2.58	4.35	4.31	4.41	3.86	4.04	4.29	4.25	4.39	4.20	4.58	4.79	4.99	5.27	5.63	5.93	6.19	3.54	3.57	3.61
Tb	0.69	0.78	0.57	0.50	0.85	0.81	0.85	0.73	0.78	0.82	0.78	0.78	0.76	0.85	0.91	0.95	0.98	1.01	1.08	1.14	0.70	0.71	0.67
Dy	4.48	5.07	3.71	3.32	5.48	5.37	5.76	4.65	5.18	5.44	4.96	5.09	4.94	5.54	5.72	5.98	6.21	6.49	6.92	7.43	4.39	4.41	4.29
Ho	0.92	1.08	0.78	0.71	1.19	1.13	1.23	0.99	1.08	1.18	1.09	1.10	1.08	1.19	1.24	1.32	1.39	1.41	1.51	1.59	0.99	1.01	0.91
Er	2.58	2.96	2.29	2.05	3.40	3.26	3.51	2.91	3.14	3.37	3.35	3.35	3.32	3.56	3.78	3.92	4.19	4.34	4.60	4.87	2.81	2.85	2.65
Tm	0.412	0.461	0.373	0.334	0.531	0.510	0.549	0.458	0.482	0.501	0.484	0.470	0.480	0.504	0.521	0.553	0.584	0.611	0.647	0.698	0.422	0.427	0.393
Yb	2.52	2.80	2.33	2.05	3.33	3.24	3.42	2.83	3.01	3.19	3.08	3.06	3.04	3.29	3.43	3.62	3.79	3.89	4.11	4.34	2.74	2.77	2.62
Lu	0.359	0.391	0.323	0.303	0.479	0.465	0.488	0.413	0.429	0.460	0.476	0.462	0.473	0.508	0.512	0.529	0.556	0.566	0.584	0.606	0.410	0.418	0.376

Table 2 - (*continued*)

	(medium-Ti)								(low-Ti)			
Sample	vsk-18	*go-12	goi-2	vsi-11	vsi-12	vsi-8/4	vsi-9	*vsi-6/1	*got-6	gtc-2	gtc-1	go-9
Rock type	MB	MB	MB	MB	MB	MB	MB	MB	PB	MB	MB	MB
Location	KA19	IV13	IV13	IV12	IV11	IV7	IV9	IV3	IV13	IV13	IV13	IV13
SiO_2	48.71	49.56	49.70	50.29	49.83	50.43	48.88	46.59	51.93	52.11	53.31	51.99
TiO_2	1.28	0.85	0.92	1.02	1.18	1.27	1.30	1.30	0.69	0.73	0.76	0.71
Al_2O_3	15.40	15.10	15.04	14.93	14.81	14.70	14.96	13.79	15.46	15.45	15.47	15.53
Fe_2O_{3total}	9.54	10.72	9.26	9.32	11.21	11.43	10.01	10.94	8.46	8.75	8.87	8.55
MnO	0.18	0.16	0.38	0.21	0.18	0.18	0.14	0.13	0.14	0.15	0.18	0.13
MgO	7.19	6.53	10.46	7.22	6.84	6.39	6.90	6.08	5.74	6.36	6.30	5.81
CaO	9.37	7.79	3.43	8.45	8.05	7.32	9.60	13.74	7.93	8.55	5.01	7.98
Na_2O	3.86	4.70	4.88	4.21	4.52	4.63	3.97	3.07	5.15	5.06	6.19	5.01
K_2O	0.16	0.01	0.05	0.11	0.08	0.13	0.16	0.06	0.10	0.04	0.04	0.02
P_2O_5	0.10	0.10	0.10	0.13	0.16	0.17	0.14	0.14	0.09	0.08	0.08	0.08
LOI	3.82	4.06	5.88	4.03	3.11	3.75	3.89	3.97	3.79	2.96	3.29	4.11
Total	99.61	99.58	100.10	99.92	99.97	100.40	99.95	99.81	98.48	100.24	99.50	99.92
Mg#	61.6	56.4	69.9	58.8	52.6	53.2	57.7	54.6	59.4	61.8	61.6	59.7
Cs	0.3	0.1	0.6	0.3	0.2	0.2	0.1	0.1	0.3	0.2	0.5	0.4
Rb	2	1	1	1	2	3	3	1	1	1	1	1
Ba	22	57	172	105	91	96	27	34	84	94	75	80
Th	0.29	0.25	0.25	0.22	0.25	0.20	0.27	0.27	0.16	0.12	0.16	0.14
Ta	0.07	0.04	0.05	0.07	0.09	0.11	0.14	0.13	0.01	0.01	0.02	0.01
Nb	1.1	0.7	0.8	1.1	1.4	1.8	2.3	2.1	0.2	0.2	0.3	0.2
Sr	178	95	157	135	106	118	85	52	94	140	120	105
Zr	83	45	46	56	68	80	89	85	36	40	42	38
Hf	2.1	1.5	1.5	1.8	2.0	2.2	2.5	2.4	1.2	1.3	1.3	1.2
Y	24	22	22	24	26	29	31	30	17	19	20	18
Sc	37	35	33	34	35	35	43	39	37	34	33	35
V	291	285	275	285	298	308	309	322	275	270	272	273
Cr	270	90	80	86	182	210	233	131	110	170	81	131
Ni	71	45	46	49	56	68	65	56	44	56	43	49
La	2.51	1.76	1.97	2.06	2.62	3.01	3.45	3.27	1.42	1.49	1.49	1.45
Ce	8.23	5.35	6.02	6.75	7.71	8.71	10.32	9.62	4.37	4.47	4.56	4.41
Pr	1.43	0.88	0.95	1.06	1.25	1.43	1.65	1.58	0.74	0.78	0.81	0.76
Nd	7.89	5.29	5.73	6.28	7.31	7.97	9.02	8.71	4.39	4.69	4.73	4.43
Sm	2.83	1.99	2.11	2.32	2.53	2.78	3.05	2.99	1.53	1.76	1.87	1.58
Eu	1.100	0.848	0.873	0.983	1.101	1.173	1.239	1.220	0.751	0.724	0.724	0.741
Gd	3.84	2.87	2.89	3.26	3.69	3.92	4.26	4.12	2.29	2.49	2.74	2.35
Tb	0.68	0.56	0.57	0.62	0.68	0.72	0.77	0.75	0.44	0.48	0.52	0.46
Dy	4.19	3.69	3.68	3.95	4.38	4.67	5.07	3.19	3.05	3.20	3.43	3.11
Ho	0.90	0.76	0.78	0.89	0.94	1.02	1.08	1.05	0.63	0.71	0.76	0.67
Er	2.49	2.29	2.40	2.72	2.91	3.10	3.29	3.19	1.91	2.12	2.29	1.99
Tm	0.384	0.339	0.357	0.389	0.421	0.441	0.468	0.453	0.283	0.307	0.331	0.294
Yb	2.44	2.27	2.39	2.51	2.68	2.88	3.05	3.01	1.89	2.02	2.20	1.94
Lu	0.343	0.347	0.352	0.391	0.412	0.432	0.461	0.452	0.284	0.321	0.349	0.298

High LOI (2.48-6.62wt%), even after extraction of amygdal calcite, is atypical for a primary dry paragenesis and corroborates the petrographical evidence of severe alteration of the samples. The relative mobility of elements was proved by their measured concentration against Zr selected as differentiation index (not shown). Large ion lithophile elements (LILE) Cs, Rb, K, Ba and Sr show variable and selective mobilization and are not suitable for petrogenetic constraints whereas high field strength elements (HFSE) Ti, Th, Hf, Nb, Ta, P, and Y as well as all REE retain igneous inter-elemental ratios. Since the concentration of alkali elements is expected to be most affected by alteration, particularly during spilitization, the diagram of Winchester and Floyd (1977) that utilizes the ratios of immobile elements is used to classify the rocks (Fig. 4). Our samples show similar Zr/TiO_2 ratios (0.005-0.010) and due to the variable Nb/Y ratios, they are spread in the fields of alkali to subalkaline basalts. Alkali basalts (Group 1) have the highest Nb/Y ratio (1.2-1.5). Subalkaline basalts may be discriminated in the group with medium high Nb/Y ratios of 0.2-0.4 (Group 2), which is typical for modern E-MORB (Sun and McDonough, 1989) and for E-MORB from the Tethyan Ocean crust (Saccani and Photiades, 2005, Aldanmaz et al., 2008; Göncüoglu et al., 2010). Another cluster of subalkaline basalts shows continuously decreasing Nb/Y ratios (0.02-0.10) and through analysis of their spider diagrams and REE patterns (see below) can be split into Group 3 (T-MORB), a compositional spectrum of N-MOR basalts (Group 4), and IAT which, due to influence of subduction derived components, has the lowest Nb/Y ratios (0.01-0.02; Group 5).

Table 3 - Nd and Sr isotope data of basaltic rocks from the Mts. Kalnik (KA) and Ivanščica (IV) ophiolite mélange.

Sample	Location	Rock group	$^{143}Nd/^{144}Nd^{a}$	$^{147}Sm/^{144}Nd$	$^{87}Sr/^{86}Sr^{a}$	$\varepsilon_{Nd(t)}{}^{b}$	$^{87}Sr/^{86}Sr_{(t)}{}^{c}$	Time (t)*
kb-6	24, KA	1 WPAB	0.512701 (12)	0.13986	0.705220 (12)	+2.94	0.705133	236 Ma
vsk-207a	5, KA	2 enr. E-MORB	0.512849 (06)	0.17565	0.705182 (06)	+4.74	0.704640	230 Ma
h-33	6, KA	2 dep. E-MORB	0.512900 (08)	0.19176	0.704889 (08)	+5.26	0.704519	230 Ma
ke-2	26, KA	3 T-MORB	0.512977 (16)	0.19639	0.704277 (16)	+6.63	0.703927	225 Ma
ja-2	4, KA	3 N-MORB	0.512999 (06)	0.21296	0.704182 (06)	+6.58	0.703142	225 Ma
vsi-6/5	3, IV	4 SSZ N-MORB	0.512961 (06)	0.20017	0.704277 (10)	+6.23	0.703776	165 Ma
h-26	8, KA	5 medium-Ti IAT	0.512981 (05)	0.21549	0.704254 (05)	+6.30	0.704193	160 Ma
got-6	13, IV	5 low-Ti IAT	0.512976 (11)	0.21072	0.704274 (10)	+6.31	0.704211	155 Ma

Location number corresponds to the locations in Fig. 1B-C. Legend: WPAB = within-plate alkali basalts (Group 1), E-MORB = enriched mid-ocean ridge basalts (Group 2), T-MORB = transitional mid-ocean ridge basalts (Group 3), N-MORB = normal mid-ocean ridge basalts (Group 4), IAT = island-arc tholeiites (Group 5); enr. = enriched, dep. = depleted, SSZ = supra-subduction zone. [a]Errors in brackets for Nd and Sr isotopic ratios are given at the 2σ-level. $^{147}Sm/^{144}Nd$ calculated from the ICP-MS concentrations of Sm and Nd following equation: $^{147}Sm/^{144}Nd = (Sm/Nd)*[0.53151+0.14252*^{143}Sm/^{144}Nd]$. [b] Initial $\varepsilon_{Nd(t)}$ calculated assuming $I^{o}_{CHUR} = 0.512638$, $(^{147}Sm/^{144}Nd)^{o}_{CHUR} = 0.1966$, and $\lambda_{Sm} = 6.54*10^{-12}$ a^{-1}. [c] $^{87}Sr/^{86}Sr_{(t)}$ calculated using ICP-MS Rb and Sr concentrations and assuming $\lambda_{Rb} = 1.42*10^{-11}$ a^{-1}. *Coresponding time for the initial ε_{Nd} and initial isotopic ratios for Sr.

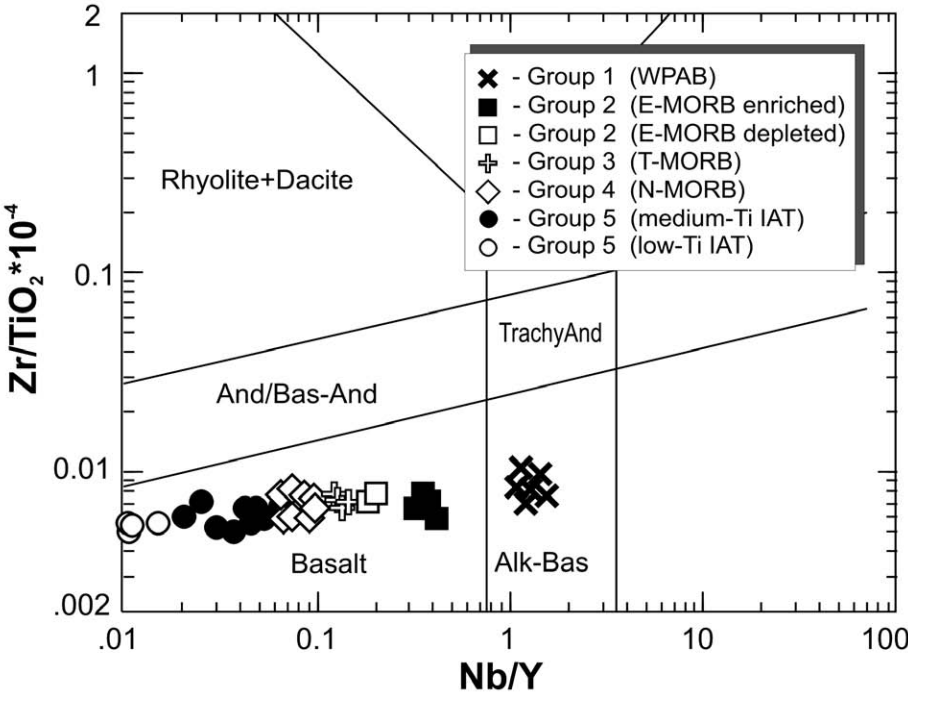

Fig. 4 - Nb - Zr/TiO_2*10^{-4} classification diagram (Winchester and Floyd, 1977) for the extrusive rocks from the Mts. Kalnik and Ivanščica ophiolite mélange.

Group 1 (WPAB-type) contains seven samples of WPAB exposed only within the Mt. Kalnik ophiolite mélanges (Table 2). Due to severe alteration of the major elements except for TiO_2 (1.58-2.42wt%) and P_2O_5 (0.30-0.58wt%), the alkaline signature of the rock is difficult to recognize. The Mg# ranging from 77.3 to 45.7 may suggest a primitive to slightly evolved composition. A Ti/V ratio of around 50 is atypically low for WPAB, and it is similar to analogous rocks from the Mt. Medvednica ophiolite mélange (Fig. 5); the Mt. Samoborska Gora WPAB are apparently more primitive. The normalized incompatible element abundance in the spider diagram from Th to Lu is characterized by a smooth pattern with slightly pronounced positive P and Ta-Nb anomalies [e.g., $(Nb/La)_n = 1.38$-1.81] and continuously decreasing abundance of the less incompatible elements. All these signatures are fairly comparable with those of WPAB from the East African rift zone (Fig. 6A1) and closely resemble patterns of ocean island basalts (OIB) (e.g., Sun and McDonough, 1989). Selective mobilization of Cs, Ba, Rb, K and Sr are due to devitrification of the glassy matrix and/or to albitization. REE patterns of the analyzed rocks display moderate LREE/HREE enrichment $[(La/Lu)_{cn} = 5.9$-$7.2]$ compared to the WPAB standard (Fig. 6B1), which is also slightly lower than the enrichment of the Mt. Samoborska

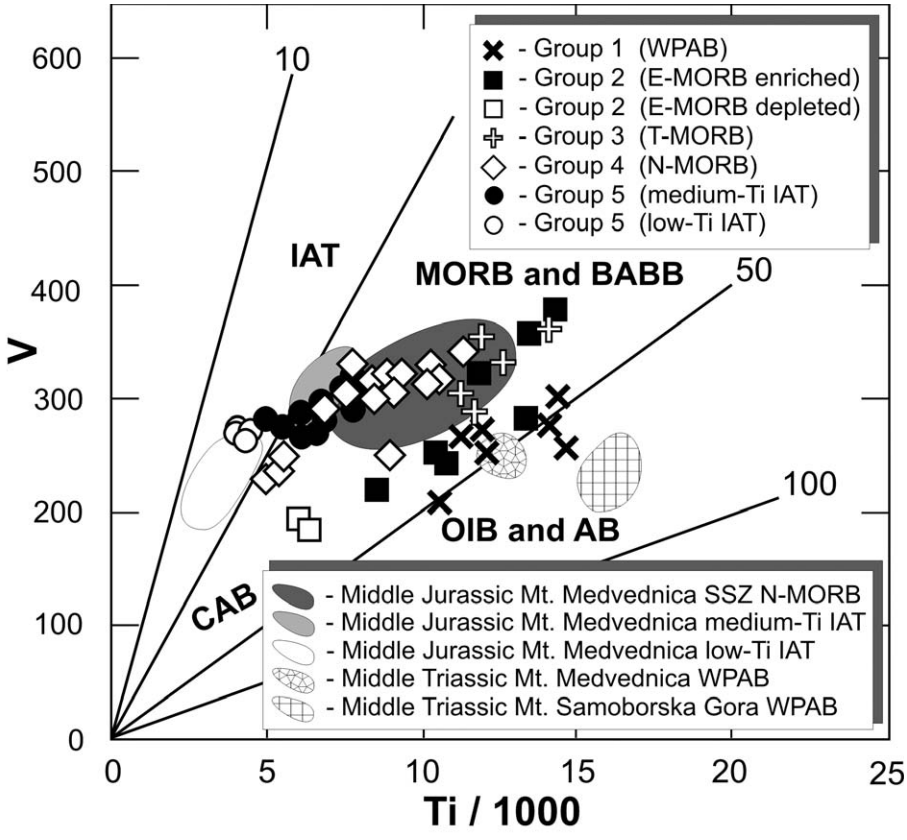

Fig. 5 - V - Ti/1000 discrimination diagram (Shervais, 1982) for the extrusive rocks from the Mts. Kalnik and Ivanščica ophiolite mélange. IAT- island-arc tholeiites, MORB- mid-ocean ridge basalts, BABB- back-arc basin basalts, CAB- calc-alkaline basalts, OIB- ocean-island basalts and AB- alkali basalts. Fields for basalts from the Mts. Medvednica and Samoborska Gora ophiolite mélange (Slovenec and Lugović, 2009; Slovenec et al., 2010) plotted for correlation constraints.

Gora alkali basalts (Slovenec et al., 2010). All analyzed alkali basalts, excluding sample vsk-234, have $Lu_n < 1$ which may indicate residual garnet in the source. In a Mt. Kalnik alkali basalt, the initial $\varepsilon_{Nd(T=236\ Ma)\ of}$ +2.96 and $(^{87}Sr/^{86}Sr)_i$ ratio of 0.705133 reveal the most depleted Nd-Sr isotopic characteristics of the Kalnik Unit alkali basalts, which all plot close to Bulk Silicate Earth (BSE; Fig. 7).

Group 2 (E-MORB-type) displays Ti/V ratios ranging from 32 to 48 and spreads in the fields of recent MORB and BABB (back-arc basin basalts) as two separate trends (Fig. 5). One set of samples shows variation trends similar to alkali basalts while another fits the trend of tholeiitic basalts at its most enriched segment. Their normalized multielement concentration patterns are displayed in Fig. 6A2 where enriched and depleted varieties are distinguished by overall lower concentrations of all immobile elements and a lower Ta-Nb anomaly $[(Nb/La)_n]$ relative to La (1.19-1.35 vs 0.98-1.01) in the latter. Relative enrichment of LILE and Sr in depleted extrusive rocks are due to alteration and albitization, respectively. The enriched rocks of Group 2 show smooth and parallel REE normalized patterns with continuous LREE/HREE enrichment $[(La/Lu)_{cn}$ = 2.4-2.6] which is significantly higher than in depleted samples $[(La/Lu)_{cn}$ = 1.4-1.5] (Fig. 6B2). The initial ε_{Nd} and $(^{87}Sr/^{86}Sr)_i$ calculated for an arbitrary age of 230 Ma range from +4.74 and 0.704640 to +5.26 and 0.704519 for relatively enriched and depleted compositions, respectively. Position of E-MORB-type basalts in the Nd-Sr initial ratios diagram suggests a mantle source with isotopic characteristics mixed between OIB- and N-MORB-type (Fig. 7).

Group 3 (T-MORB-type) and Group 4 (N-MORB-type) basalts spread in the field of recent MORB and BABB but are separated by different Ti/V ratios ranging from 31-40 and 23-33, respectively (Fig. 5).

Group 3 basalts clearly show transitional geochemical signature towards the E-MORB-type of Group 2. Transitional chemistry of these basalts is also indicated in their spider diagram (Fig. 6A3) by the slightly inclined profile from Th to Lu $[(Th/Lu)_n$ = 3.2-3.6] at a concentration level of 1.8 to 2.9 times relative to N-MORB. The Mg# of these transitional basalts ranges from 57.9 to 67.8 and is significantly higher than in the analyzed N-MOR-type basalts (50.4-67.0), arguing against their significant fractionation. Group 3 basalts show an insignificant Ta-Nb negative anomaly $[(Nb/La)_n$ = 0.91-0.96] that is not uncommon in Dinaric ophiolite MORB-type extrusives (Lugović et al., 1991; Trubelja et al., 1995); however the intensity of the anomaly is fairly low when compared to all the analyzed ophiolitic rocks. The transitional basalts display convex REE patterns at 17-20 times relative to chondrite, and show slight LREE/MREE depletion $[(La/Sm)_{cn}$ = 0.79-0.87] and MREE/HREE enrichment $[(Sm/Lu)_{cn}$ = 1.24-1.40] (Fig. 6B3). The Eu anomaly of Group 3 basalts (Eu/Eu* = 0.93-1.03) is typical for low accumulation or fractionation of plagioclase. Nd-Sr isotopic signatures of T-MORB $[\varepsilon_{Nd(T=225\ Ma)}$ = +6.63; $(^{87}Sr/^{86}Sr)_i$ = 0.703927] follow the depletion trend of enriched non-mantle array sources reflected by rocks of Groups 1 and 2 (Fig. 7).

The basalts of Group 4 reveal a broad variety of N-MORB-type compositions by their multi-element abundance patterns shown in their spider diagram (Fig. 6A3) and REE patterns (Fig. 6B3) suggesting a high fractionation span and/or successively different sources for magma genesis. In the spider diagram all rocks of this group show an inconsistent secondary LILE enrichment and a slightly flat profile from La to Lu $[(La/Lu)_n$ = 1.15-1.66] at a concentration level of 0.6 to 2.6 times relative to N-MORB, which is

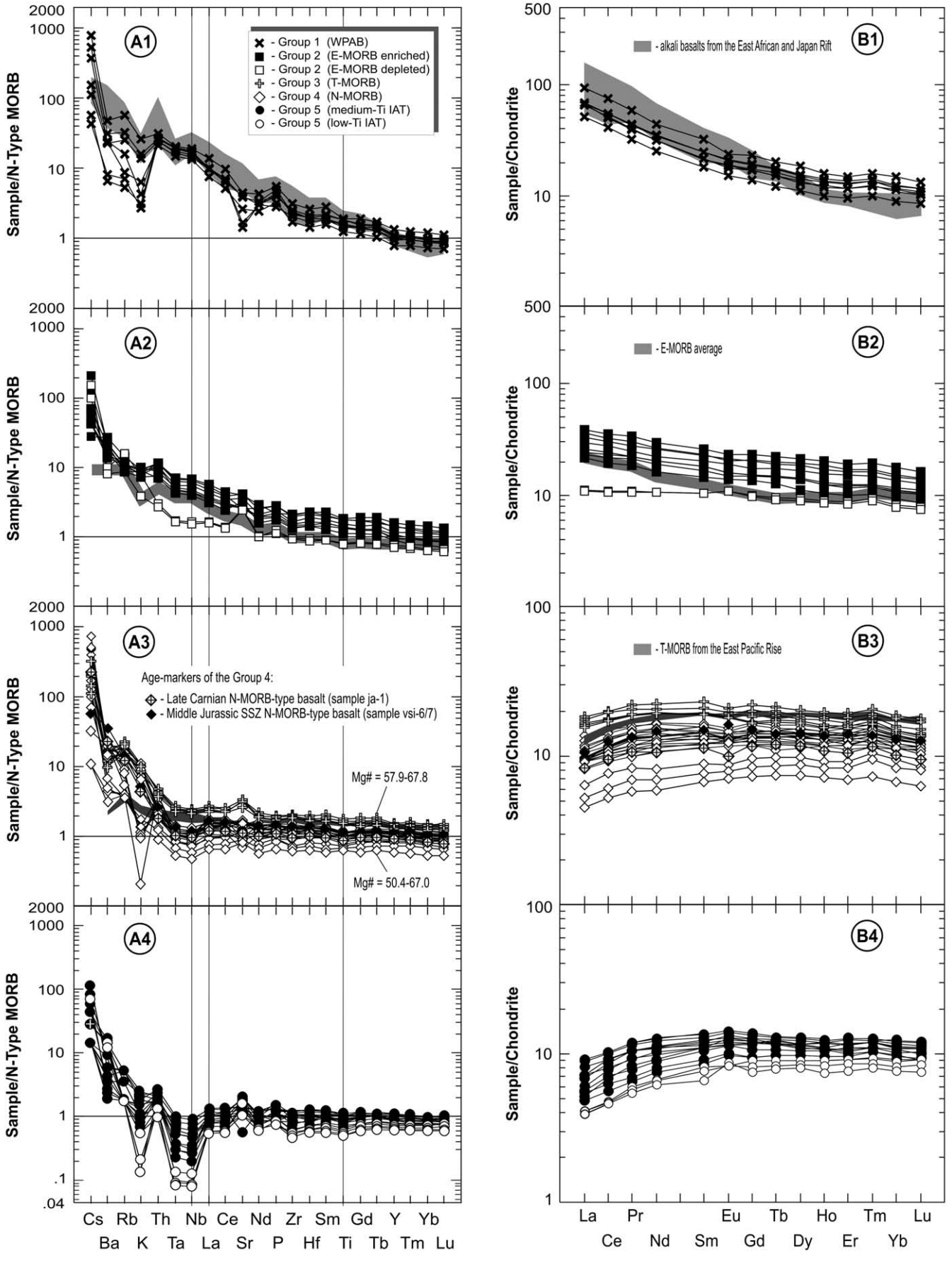

Fig. 6 - (A) N-MORB-normalized (Sun and McDonough,1989) multielement patterns and (B) REE-normalized (Taylor and McLennan, 1985) patterns for the Mts. Kalnik and Ivanščica extrusive rocks. Field for alkali basalts from the East African Rift-Kenya Rift (Wilson, 1989; Spath et al., 2001), Japan Rift (Okamura et al., 2005), E-MORB (Sun and McDonough, 1989) and T-MORB from the East Pacific Rise (Geshi et al., 2007) are shown for comparison.

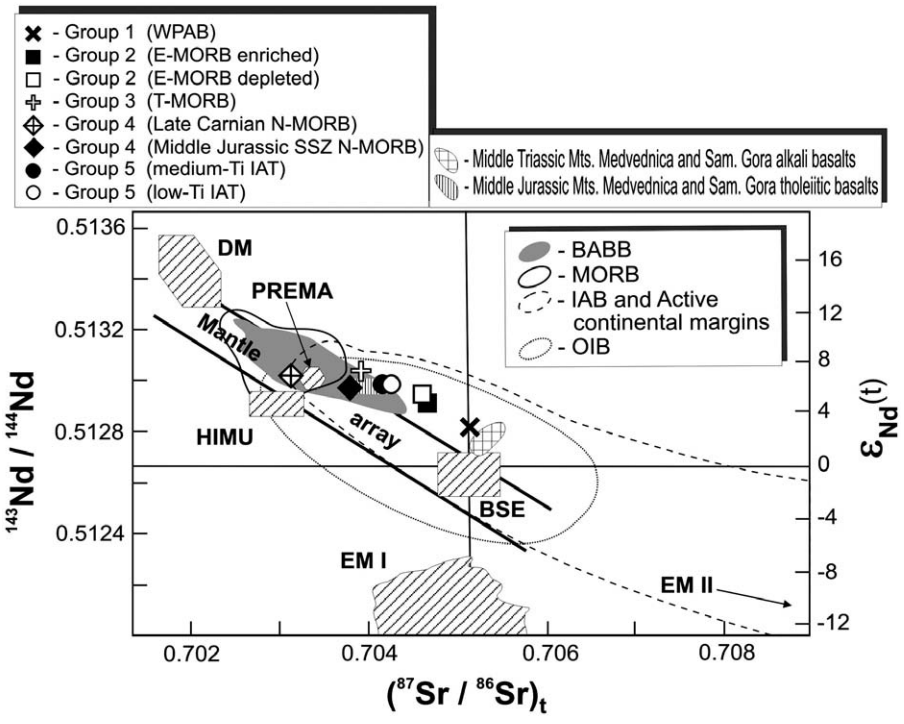

Fig. 7 - Initial $^{143}Nd/^{144}Nd$ - $^{87}Sr/^{86}Sr$ isotope ratios diagram for the Mts. Kalnik and Ivanščica extrusive rocks and Mts. Medvednica (Slovenec and Lugović, 2009) and Samoborska Gora (Slovenec et al., 2010), showing the main oceanic mantle reservoirs of Zindler and Hart (1986). DM- depleted mantle, BSE- bulk silicate Earth, EMI and EMI II- enriched mantle, HIMU- mantle with high U/Pb ratio, PREMA- frequently observed PREvalent MAntle composition. The mantle array is defined by many oceanic basalts and a bulk Earth value for $^{87}Sr/^{86}Sr$ can be obtained from this trend. Data for back-arc basin basalts - BABB (shaded field) compiled from Wilson (1989), Cousens et al. (1994), Pearce et al. (1995), Gribble et al. (1998) and Ewart et al. (1998). Data for mid-ocean ridge basalts - MORB (solid line) compiled from Wilson (1989),, Cousens et al. (1994) and Peate et al. (1997). Data for oceanic island arcs and active continental margins - IAB (broken line) compiled from Wilson (1989), Cousens et al. (1994), Pearce et al. (1995) and Peate et al. (1997).

significantly lower compared to the related T-MORB-type rocks. A slight to significantly pronounced HFSE anomaly is obvious in all samples (Fig. 6A3). The anomaly is expressed as $(Nb/La)_n$ in the representative late Carnian age-marker (Fig.1B; sample ja-1, location 4) and Middle Jurassic SSZ basalt from the composite block (Fig.1C; sample vsi-6/7, location 3) is 0.81 and 0.72, respectively. This may suggest a continuous decrease of the subduction influence due to onset of ocean spreading, as already indicated by the Bajocian-Bathonian N-MORB-type basalts from the adjacent Mt. Medvednica ophiolite mélange (Slovenec et al., 2009), and the subsequent re-establishment of the subduction related influence during intraoceanic convergence. The REE patterns show similar profiles to the group of T-MORB-type basalts but with very wide compositional variations which range 7-20 times relative to chondrite (Fig. 6B3). The basalts display a relatively low LREE depletion $(La/Sm)_{cn}$ = 0.67-0.87) and a nearly flat HREE profile [$(Tb/Lu)_{cn}$ = 1.06-1.34]. Concerning Nd-Sr isotopic compositions, the N-MORB-type extrusives resemble the first rocks of the Kalnik Unit magmatic succession with pure mantle-array geochemical signatures (Fig. 7). Their Late Triassic age-marker with $\varepsilon_{Nd(T=225\ Ma)}$ = +6.58 and $(^{87}Sr/^{86}Sr)_i$ = 0.703142 and Middle Jurassic age-marker showing $\varepsilon_{Nd(T=165\ Ma)}$ = +6.23; $(^{87}Sr/^{86}Sr)_i$ = 0.703776 clearly reflect re-fertilization of the mantle source for the latter, most likely by subduction related fluids.

Group 5 (IAT-type basalts) displays Ti/V ratios ranging from 15-17 in the low-Ti samples, to 18-26 in the medium-Ti samples, and consequently form a continuous trend from the IAT to MORB/BABB fields (Fig. 5). The SSZ lavas with IAT affinity are successfully discriminated from the associated N-MORB-type lavas (which are ordinarily high-Ti) on the basis of the TiO_2 content (Bortolotti et al., 2002). Medium-Ti (0.7-1.3wt% TiO_2) and low-Ti (0.29-0.76wt% TiO_2) IAT lavas may suggest formation at various stages in a SSZ setting. (Serri, 1981; Beccaluva et al., 1983). In the spider diagram the rocks of this group show inconsistent LILE enrichment and a flat pattern for the more incompatible and immobile elements in the segment from La to Lu which ranges from 0.8 to 1.5 times relative to N-MORB for the medium-Ti basalts and 0.5-0.8 times for the low-Ti basalts (Fig. 6A4) - consistent with their degree of depletion. All rocks show a pronounced negative anomaly of HFS elements, whose intensity significantly increases from medium-Ti basalts [$(Nb/La)_n$ = 0.24-0.72] to low-Ti basalts [$(Nb/La)_n$ = 0.12-0.22], suggesting more subduction related signatures of the latter. These geochemical signatures are widely accepted as typical of IAT that is, suprasubduction basalts (e.g., Pearce, 1984; Weaver and Tarney, 1984). The normalized REE patterns of the basalts show nearly flat HREE profile [$(Tb/Lu)_{cn}$ = 0.98-1.17] at 9-13 times relative to chondrite for the medium-Ti group and 8-9 for low-Ti group and various intensities of LREE depletion (Fig. 6B4). The intensity of LREE depletion decreases from medium-Ti basalts [$(La/Sm)_{cn}$ = 0.54-0.71] to low-Ti basalts [$(La/Sm)_{cn}$ = 0.50-0.58] which also indicates the overall more depleted nature of the low-Ti basalts. The initial $\varepsilon_{Nd\ (T=\ 160\text{-}155\ Ma)}$ and $(^{87}Sr/^{86}Sr)_i$ for two IAT basalts are very consistent: +6.30-6.31 and 0.704193-0.704211. Along with the Middle Jurassic SSZ N-MORB-type basalts from Group 4 associated with the composite block, they provide evidence for the successive enrichment of a joint source through subduction related components (Fig. 7).

K-Ar AGES

K-Ar isotopic analyses were performed on three basaltic samples and the results are presented in Table 4. The calculated ages are interpreted as the ages of rock consolidation. A bulk rock from an alkali WPB of Group 1 showed a consolidation age of 243-229 Ma, which in the geologic time scale of Ogg (2004) corresponds to middle Anisian-late

Table 4 - K-Ar plagioclase whole rock ages of extrusive rock from from the Mts. Kalnik (KA) and Ivanščica (IV) ophiolite mélange.

Sample	Location	Rock group		K [%]	^{40}Ar (rad) ccSTP/g	^{40}Ar (rad) [%]	Age Ma ± 1σ
vhk-11, wr	21,KA	WPAB	1	0.411	6.563×10^{-7}	14.44	235.8 ± 7.1
h-26, pl	8, KA	medium-Ti IAT	5	0.132	9.349×10^{-7}	43.61	164.7 ± 6.4
got-6, wr	13, IV	low-Ti IAT	5	0.139	8.481×10^{-7}	23.35	154.7 ± 8.7

Location number corresponds to the locations in Fig. 1B-C.
Legend: WPAB = within-plate alkali basalts (Group 1); IAT = island-arc tholeiites (Group 5); pl = plagioclase separate; wr = bulk rock.

Ladinian. A plagioclase separate from an IAT-type medium-Ti basalt of Group 5 yielded an age of 170-158 Ma, which corresponds to early late Bajocian-middle Oxfordian, consistent with the late Bajocian-Callovian age of radiolarian fauna from associated cherts (Goričan et al., 2005); an IAT-type low-Ti pillow basalt from Group 5 showed an age span of 163-146 Ma which corresponds to middle Callovian-late Tithonian.

DISCUSSION AND CONCLUSIONS

An ophiolite mélange reflects a polyphase history and records a variety of tectono-sedimentary processes from deposition in an accretionary wedge to onset of thrusting onto a passive continental margin. Through deposition and subsequent thrusting various fragments of the oceanic basin unrelated in terms of time and setting may be juxtaposed in the resulting mélange. Some lithologies found in an ophiolitic mélange are not found in the sequence of the associated ophiolite and therefore that is the only prove of their existence in the related oceanic segment. The Mts. Kalnik and Ivanščica ophiolite mélanges that form the unique northern segment of the Kalnik Unit include juxtaposed basaltic fragments of five distinct geochemical groups that show significant inter-group geochemical variations. They are defined as: Group 1 (non-orogenic alkali WP basalts of uniform composition), Group 2 (various E-MORB-type basalts), Group 3 (T-MORB-type basalts), Group 4 (a series of N-MORB-type basalts) and, Group 5 (a series of IAT-type basalts), which indicates the non-uniform origin of their magma in different tectonic settings and ages of crystallization. On the contrary, rare composite blocks composed of N-MORB-type and IAT-type basalts reflect a relatively uniform origin and age of two different types of magmatism. The Mt. Kalnik sector of the Kalnik Unit contains fragments of all groups (Groups 1-3 are statistically most abundant) while the Mt. Ivanščica sector incorporates only ophiolitic basalts from Groups 4 and 5, suggesting that the ophiolitic mélange during accretion may be tectonically differentiated into sectors at the onset of obduction.

Tectonomagmatic significance of Group 1 basalts (WPAB-type)

Blocks of alkaline basaltic rocks in ophiolite mélanges have been interpreted as remnants of OIB or seamounts built in oceanic crust through intra-plate hot spot magmatism (Rojay et al., 2001; 2004; Saccani and Photiades, 2005; Gökten and Floyd, 2007; Monjoie et al., 2008). Alkali basalts related to intracontinental rift volcanism (CRB) closely preceding the formation of oceanic crust have a composition similar to OIB (Fitton, 2007); such basalts from the eastern Mediterranean Mesozoic mélanges are thought to represent within-plate volcanism that took place during the onset of continental break-up before the initial oceanic crust formed (Bortolotti et al., 2009; Koglin et al., 2009).

Alkali basalts from the Mt. Kalnik ophiolite mélanges with $(Th/Lu)_n$ ratios of 27-31 show a slightly depleted composition compared to the Mt. Medvednica analogues [$(Th/Lu)_n$ = 32-46; Slovenec et al., 2010], and are significantly more depleted than the ordinary OIB and Mt. Samoborska Gora alkali basalts (Fig. 8A). Several samples characterized by the lowest relative abundance of HREE ($Lu_{cn} < 10$) in Fig. 6B1 may reflect paragenetic garnet in the related mantle source (Spath et al., 2001). Agrawal et al. (2008) succeeded to discriminate OIB and CRB compositions by the multielement ratios discriminating function. All alkali basalts from the Kalnik Unit plot in the field defined for CRB at an 85% confidence level (Fig. 8D). Fairly similar and uniform compositions of Mts. Kalnik and Medvednica alkali basalts suggest that they derived from a similar source which shows Nd-Sm isotopic composition slightly more depleted than BSE (Fig. 7). Assuming that all alkali basalts from the Kalnik Unit shared the same or similar source, then a kind of partial melt succession of alkali basalts from Mts. Samoborska Gora via Medvednica to Kalnik may be inferred from the depletion trend of Nd-Sm isotope compositions. This means that Mt. Kalnik should reflect the youngest alkali basalt volcanism in the ROD, albeit their isotopic ages (235.8±8 Ma) span from middle Anisian to late Ladinian. This fact may support the idea deduced from the rock geochemistry that these alkali basalts are not ophiolitic rocks but represent instead intracontinental rift magmatism. If this statement is correct, then extensive lithospheric extension must have occurred, due to upwelling of subcontinental asthenospheric mantle in the ROD during the Middle Triassic. The low La/Ta ratio (9.5-12.4) of the analyzed alkali basalts is typical for uncontaminated CRB (Hart et al., 1989), suggesting that the basalts erupted through highly attenuated continental crust, probably in the terminal stage of its extension.

The Mt. Kalnik alkali basalts correspond to the melts extracted from an OIB-type mantle source (Fig. 8A). Haase and Devey (1996) proposed a model based on interelement

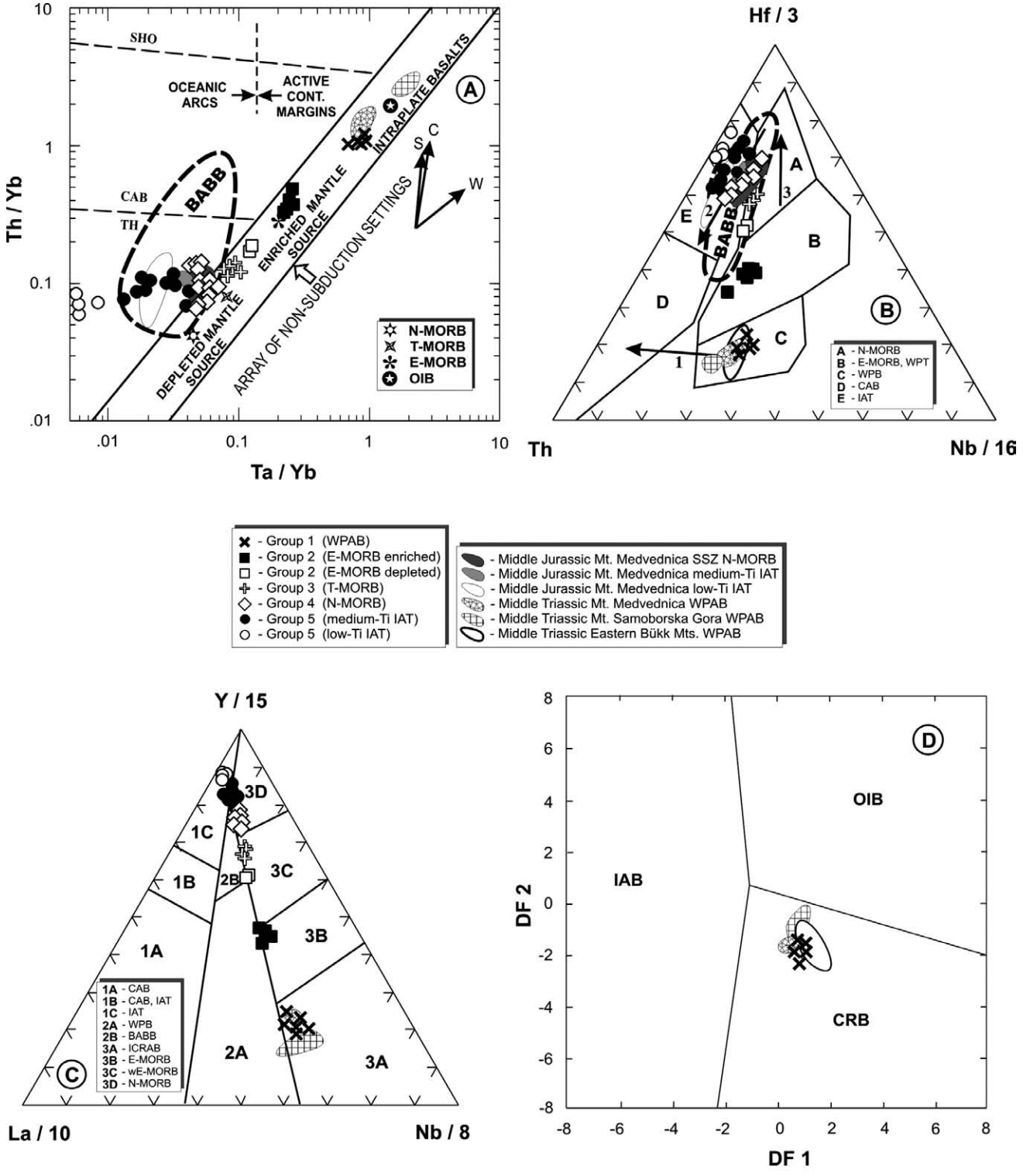

Fig. 8 - Discrimination diagrams for the extrusive rocks from the Mts. Kalnik and Ivanščica ophiolite mélange. (A) Ta/Yb - Th/Yb diagram (Pearce, 1983). S- subduction zone enrichment; C- crustal contamination; W- within-plate enrichment. N-MORB, E-MORB and OIB are from Sun and McDonough (1989). T-MORB are from Geshi et al. (2007). Data for back-arc basin basalts (BABB) fields are from Pearce et al. (1984), Ewart et al. (1994) and Leat et al. (2000). (B) Th - Nb/16 - Hf/3 diagram (Wood, 1980). A- normal mid-ocean ridge basalts (N-MORB); B- enriched MORB (E-MORB) and within-plate tholeiites (WPT); C- alkaline within-plate basalts (AWPB); D- calc-alkali basalts (CAB); E- island-arc tholeiites (IAT); 1- crustal contamination; 2- SSZ ophiolites trend; 3- MORB ophiolites trend. Data for back-arc basin basalts (BABB) compiled from Saunders and Tarney (1979), Weaver et al. (1979), Craford and Keays (1987), Jahn (1986), Ikeda and Yuasa (1989), Ewart et al. (1994), Gribble et al. (1998), Leat et al. (2000) and Münker (2000). (C) La/10 - Nb/8 - Y/15 diagram (Cabanis and Lecolle, 1989). 1- volcanic arc basalts; 2- continental basalts; 3- oceanic basalts; 1A- calc-alkali basalts (CAB); 1B- calc-alkali basalts and island-arc tholeiites (CAB, IAT); 1C- island-arc tholeiites (IAT); 2A- within-plate basalts (WPB); 2B- back-arc basin basalts (BABB); 3A- intercontinental rift alkali basalts (ICRAB); 3B- enriched MORB (E-MORB); 3C- weakly enriched MORB (E-MORB); 3D- normal mid-ocean ridge basalts (N-MORB). (D) DF_1 - DF_2 diagram (Agrawal et al., 2008; $DF_1 = 0.5533 \log_e (La/Th) + 0.2173 \log_e (Sm/Th) - 0.0969 \log_e (Yb/Th) + 2.0454 \log_e (Nb/Th) - 5.6305$; $DF_2 = -2.4498 \log_e (La/Th) + 4.8562 \log_e (Sm/Th) - 2.1240 \log_e (Yb/Th) - 0.1567 \log_e (Nb/Th) + 0.94$). IAB- island-arc basalts; OIB- ocean-island basalts; CRB- continental rift basalts. Fields for basalts from the Mts. Medvednica and Samoborska Gora ophiolite mélange (Slovenec and Lugović, 2009; Slovenec et al., 2010) plotted for correlation constraints.

ratios of REE which is useful to identify a mantle source for different types of related magmas. From the $(Dy/Yb)_n$ - $(Ce/Yb)_n$ diagram it is evident that the analyzed basaltic rocks from Groups 1-5 Mts. Ivanščica and Kalnik represent melts related to three different mantle sources (Fig. 9). The analyzed alkali basalts from Mt. Kalnik derived from a pure plume mantle source which experienced ~ 5-6% total partial melting, slightly higher than that for the Mt. Medvednica mantle source. The lowest intensity of partial melting of a similar source (around 4%) is found in alkali basalts from the Mt. Samoborska Gora ophiolite mélange.

Tectonomagmatic significance of Group 2 basalts (E-MORB-type)

In the Mt. Kalnik ophiolite mélange distinct E-MORB-type basalts were recognized, with both relatively enriched and depleted compositions (Table 2, Fig. 8A-C). Enriched E-MORB-types are primarily associated with pelagic cherts of early Ladianian age, while depleted varieties are interlayered with radiolarian chert of late Ladinian age. Since E-MORB-type basalts coincide in age with the alkali basalts, they most likely either erupted at the continental edge as the last alkali volcanic rocks, or closely succeeded the eruption of the alkali basalts which may reflect the initial succession of oceanic protocrust formation.

E-MORB-type magmas are known from different oceanic settings as well as from continental rift zones. For ophiolites, the initial E-MORB magma may be generated from slightly enriched mantle sources or by low degree partial melting of depleted N-MORB-type sub-oceanic mantle sources (Saccani and Photiades, 2005; Bortolotti et al., 2009). A Ta/Yb vs Th/Yb plot of Group 2 basalts indicate that the enriched varieties are slightly more enriched compared to the recent primitive E-MORB of Sun and McDonough (1989) while the depleted varieties tend towards N-MORB-type compositions (Fig. 8A). Isotopic compositions of E-MORB-type basalts from the Kalnik Unit indicate an enriched mantle source mixed with OIB and N-MORB-type components (Fig 7) which suggest mixing and, also two successive stages of partial melting and magma generation at a spreading ridge activated during the proto-oceanic stage. Relatively enriched E-MORB-type oceanic crust was produced during the older (early Ladianian) magmatic stage, and depleted E-MORB-type crust was generated during the younger (late Ladinian) stage. The older stage basalts perfectly match the inferred melting curve for the mixed plume/MORB mantle source of Haase and Devey (1996) which experienced total partial melting of 9.3 to 11% (Fig. 9). However, the younger stage basalts reflect melts derived from an already depleted mixed source which is significantly influenced by MORB-source components. Alternatively, enriched and depleted E-MORB-type basalts may share a common mantle source, where the latter represent melts produced by a higher degree of partial melting.

Tectonomagmatic significance of Group 3 (T-MORB-type) and Group 4 (N-MORB-type) basalts

The rocks of Group 3 are more depleted with respect to E-MORB depleted varieties and generally show compositions transitional to basalts of Group 4 (Fig. 6, 7 and 8); therefore, they can be recognized as a distinct geochemical group of rocks. Their age-markers reveal a middle Carnian age of crystallization (Fig. 1B, location 26, samples ke-2 and ke-15) that closely precedes the late Carnian age of the associated blocks of basalts from Group 4, which represent the oldest documented N-MORB-type spreading ridge rocks in the ROD. A modern T-MORB analogue from the East Pacific Rise (EPR) may erupt close in time to the N-MORB basalts along a single section of the ridge (Reynolds et al., 1992,) as a consequence of variable OIB-type plume interaction with depleted suboceanic mantle (Haase, 2002). According to Geshi et al. (2007) the T-MORB lavas at the EPR

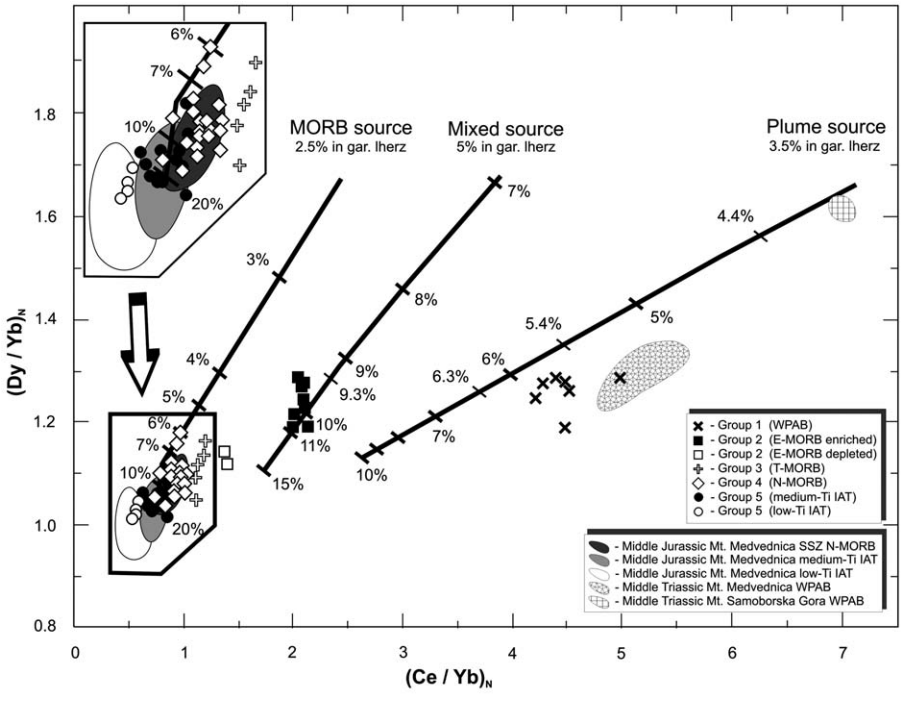

Fig. 9 - $(Dy/Yb)_N$ - $(Ce/Yb)_N$ diagram and partial melting model (Haase and Devey, 1996) for mafic extrusive rocks from the Mts. Kalnik and Ivanščica ophiolite mélange. The melt model for accumulated batch melting using 1% melt steps. Kds and MORB source are from McKenzie and O'Nions (1991). The plume source has 2.2 ppm Ce, 0.55 ppm Dy and 0.35 ppm Yb, the mixed source for enriched tholeiites has 1.7 ppm Ce. Melting starts with residual garnet and continues in the spinel lherzolite field. Fields for basalts from the Mts. Medvednica and Samoborska Gora ophiolite mélange (Slovenec and Lugović, 2009; Slovenec et al., 2010) plotted for correlation constraints.

are formed by mixing of depleted N-MORB magmas with enriched E-MORB magmas, which arrived to a joint shallow reservoir from discrete source regions where they mixed before the eruption; otherwise the two discrete magmas would crystallise in separate magma-types. The T-MORB-type blocks from the Mt. Kalnik ophiolite mélange show overall geochemical signatures which fit the EPR T-MORB compositions as epitomized by their Zr/Nb ratios of ~ 27 and $(La/Yb)_n$. of 1.7-1.9. However, Mt. Kalnik T-MORB-type basalts are slightly more LREE enriched (Fig. 6B3) consistently with their more primitive nature (Fig. 6A3, Fig. 8A) which is also seen through their slightly higher Sr isotope compositions compared to the EPR T-MORB of Geshi et al. (2007). Our data suggest that the T-MORB-type extrusives generated at the well established spreading center via mixing of magmas derived from two sources, a MORB source which dominates, and a mixed source (Fig. 9) which underwent an earlier extraction of E-MORB-type melts. The very homogeneous chemical compositions of Group 3 basalts indicate a short stage of T-MORB magma production during the middle Carnian in the ROD. Low volume T-MORB lavas generated in a relatively short period suggests a low degree of partial melting reflected in the LREE enriched nature of these rocks (Fig. 6B3). In mélanges from the Dinaride/Albanide-Hellenide ophiolite belts analogous basalts are assumed to be related to melts derived from a similar mantle type, as documented for modern oceanic equivalents (Pe-Piper, 1998).

Basalts of Group 4 are mostly represented as a chemographically homogeneous block in both northern sectors of the Kalnik Unit (Fig. 1B-C). The age-marker of Group 4 (Fig. 1B, location 4; sample ja-1) yielded a Late Carnian age. However, composite blocks including Group 4 and Group 5 extrusives, that is, N-MORB-type and IAT-type basalts, may be very seldom encountered in the Mt. Ivanščica sector (Fig. 1C, location 3, samples vsi-6/5-7 and vsi-6/1, respectively). In the southern sectors of the Kalnik Unit in the Mts. Medvednica and Samoborska Gora, similar composite olistoliths are relatively abundant (Slovenec and Lugović, 2009; Slovenec et al., 2010) and are interpreted as remnants of upper plate (SSZ) magmatism during the late Bathonian to early Oxfordian convergence (Slovenec and Lugović, 2009).

Group 4 extrusives are essentially N-MORB-type basalts and reflect a spectrum of compositions corresponding to the degree of partial melting from a similar source and/or fractionation of the extracted melts (Fig. 6A3 and 6B3). The basalt suite of this group derives from a MORB-type mantle source that experienced partial melting from 6 to 20% (Fig. 9). A slight to pronounced deficiency of HFSE in the N-MORB-type basalts, illustrated by the Ta-Nb relative abundance (Fig. 6A3) and their continuous shift to subduction related tholeiitic basalt compositions (Fig. 8A-C) suggest that the initial mantle source must have been inherited by some amount of subduction related components. The amount of the inherited subduction component decreases from the late Carnian N-MORB-type basalt [$(Nb/La)_n$ = 0.81], related to an already evolved spreading ridge, to the Bajocian-Bathonian N-MORB-type extrusive from the Poljanica Creek in the Mt. Medvednica ophiolite mélange [$(Nb/La)_n$ ~ 1; Slovenec and Lugović, 2009] which represents magmatism at the spreading ridge of an evolved ocean. This may suggest a continuous decrease of the subduction influence due to onset of ocean spreading in the ROD. However, Early Jurassic N-MORB-type volcanics in the Kalnik Unit are still waiting to be found to confirm this statement. Nd-Sr isotopic compositions of N-MORB-type age-markers differ greatly (Fig. 7). Late Carnian reper fits better to MORB composition while Middle Jurassic marker refers better to BABB composition and plots in the field of SSZ extrusives of Mts. Medvednica and Samoborska Gora (Fig. 7). The N-MORB-type extrusive (sample vsi-6/7) associated with Middle Jurassic IAT-type basalt (sample vsi-6/1) in a composite block has a low $(Nb/La)_n$ of 0.72, which suggests re-establishment of subduction components in the mantle source material. The geochemical character of this basalt type (in the tectonomagmatic sense) is best described as "MORB with arc signatures" (Shervais, 2001). The latter type of volcanics from Group 4 correspond to N-MORB-type extrusives generated off the ridge. In the Mt. Medvednica ophiolite mélange they reflect magmatism related to a subducting ridge as the incipient crust built into the upper plate (Slovenec and Lugović, 2009). It is important to stress that Late Triassic N-MORB-type spreading ridge related volcanics, which also bear the MORB-with-arc signature characteristics, and the homogeneous blocks of Middle Jurassic SSZ-related N-MORB analogues may be distinguished only by age and determination and isotopic composition.

From our data it appears that the production of N-MORB-type oceanic crust in the ROD began in late Carnian. Based on the simultaneous crystallization of T-MORB and N-MORB rocks along modern ocean ridge segments (Geshi et al., 2007) it is possible that N-MORB-type crust in the ROD was already being generated during the Middle Carnian.

Tectonomagmatic significance of Group 5 (IAT-type) basalts

The extrusives of Group 5 are found in discrete blocks, or occasionally in composite blocks along with N-MORB-type volcanics, suggesting that magmatism with diverse geochemical signatures may be contemporaneously occurring at a single geotectonic setting. Such contrasting magma association which includes N-MORB- and IAT-type rocks is very common in ophiolite slices thrust over ophiolite mélanges as seen in the Mirdita ophiolites in Albania (Bébien et al., 2000; Hoeck et al., 2002; Bortolotti et al., 2002; Dilek et al., 2007).

Group 5 basalts are split into two distinct groups, which according to the TiO_2-content classification scheme correspond to medium-Ti and low-Ti sub-groups (Bortolotti et al., 2002). The basaltic rocks display moderate to strong depletion of all HFSE, particularly Ta-Nb (Fig. 6A4) which is typical for SSZ magmatic rocks, due to the transfer of hygrophile elements from the subducting slab into the overlying mantle wedge. In the diagrams which geochemically discriminate rocks from various tectonic settings these basalts plot exclusively in the field of IAT SSZ rocks (Fig 8A-C). Although the overall intensity of depletion is higher in the low-Ti basalts compared to medium-Ti basalts (Fig. 6A4-B4), the relative element abundance of these rocks suggests derivation from a similar mantle source during successive stages of partial melting. Nd-Sr isotopic compositions of IAT-type basalts from the Kalnik Unit indicate refertilization of the mantle wedge with an isotopic signature of the source that is transitional between E-MORB and T-MORB (Fig. 7). The medium-Ti basalts derived from a mantle region experienced 8 to ~ 20% total partial melting while the low-Ti basalts derived from a mantle sector endured > 20% partial melting (Fig. 9). The slight shift of IAT-type rocks from the pure anhydrous MORB source

melting curve toward a more enriched source indicates mantle wedge metasomatism by ascending fluids. The transitional harzburgites from Gornje Orešje in Mt. Medvednica with mineral compositions consistent with ~ 20% partial melting (Lugović et al., 2007) may represent the mantle residuum of these melts. The IAT-type basalts of Group 5 are LREE depleted which is atypical compared to modern SSZ analogues. However, similar LREE depletion is reported for IAT-type basalts from many Tethyan Mesozoic ophiolites (Serri, 1981; Beccaluva et al., 1983; Beccaluva and Serri, 1988). These geochemical signatures suggest that the mantle wedge source was extremely LREE depleted before being metasomatized and therefore it was never capable of producing LREE enriched melts.

Clinopyroxene composition as a tectonomagmatic discriminatory tool

Clinopyroxene and oxide ores are magmatic phases preserved in most basaltic samples from the Kalnik Unit. Plagioclase is by rare exceptions altered to albite ± prehnite ± calcite which may redistribute diagnostic elements and disturb the original composition of igneous rocks. Therefore, clinopyroxene chemistry is utilized to characterize the original tectonomagmatic settings of host basalts, particularly for ophiolitic basalts (e.g., Beccaluva et al., 1989). Clinopyroxenes hosted in the alkali basalts are exclusively diopsides, in E-MORB-type basalts have a diopside-augite composition, while in T-MORB-type basalts they belong to augites that form the smooth Fe-enrichment trend; the majority of N-MORB-type and IAT-type clinopyroxenes are also augites, showing a scattered trend of Fe-enrichment (Fig. 2). The N-MORB-type with arc signatures - sample vhk-15 and IAT-type sample h-26 from Mt. Kalnik - contain a diopside-augite population that forms a separate trend of Fe-enrichment at elevated Wo-content. These clinopyroxenes display the most Ti-enriched compositions amongst clinopyroxenes from rock Groups 4 and 5 (Table 1). Textural evidence shows cotectic crystallization of spinel and clinopyroxene (± olivine) followed by Ti-poor magnetite in the host rock, which caused the high partition of Ti in cotectic, early crystallized clinopyroxenes. The sample vhk-15, with a bulk rock composition similar to N-MORB-type basalts with SSZ signatures, contains reversely zoned clinopyroxene indicative of the influx of hotter and more primitive melt to the magma storage. This fact may extend to the entire Kalnik Unit the statement that the basalts reflect an increased thermal regime governing the incipient crust formation in the obducted plate, as suggested for Mt. Samoborska Gora by Slovenec et al. (2010). Clinopyroxenes from alkali basalts, both the E-MORB-type and T-MORB-type plotted in Fig. 3A and N-MORB-type and IAT-type basalts in Fig. 3B form well defined trends of continuously decreasing TiO_2 at fairly a constant Si/Na ratio in both displays. Consequently, they plot in the fields competent for their chemistry found by Beccaluva et al. (1989) for analogue rocks in the Mediterranean ophiolites and in the southern segment of the Kalnik Unit (Fig. 3A-B). Clinopyroxenes from samples vhk-15 and h-26 have an anomalously high TiO_2 concentration due to the cotetic crystallization with spinel instead of magnetite and plot in the fields of E-MORB and N-MORB, respectively (Fig 3B), suggesting that such equilibrated clinopyroxenes are not useful for tectonomagmatic discrimination.

Clinopyroxene Ti/Al ratio may be used as a relative geothermobarometer in the sense that low ratios reflect increased pressure (Shiffman and Lofgren, 1982). According to the proposed statements the low-Ti IAT type basalt clinopyroxene reflects the highest pressure (Ti/Al = 0.05-0.08) while those from the alkali WP basalts with Ti/Al of 0.36-0.49 represent the lowest confined pressure. This fact is in agreement with the textural evidence of clinopyroxene preceding plagioclase crystallization in IAT-type basalts and the high amount of amygdals in the alkali WP basalts. Different types of ridge related basalts showing clinopyroxene Ti/Al ratio ranging randomly from 0.11 to 0.35 suffered intermediary pressure which is consistent with the ophitic to intergranular textures of most samples.

Integrated geodynamic evolution of the ROD

The ROD belongs to the easternmost segment of Neotethys (Bortolotti and Principi, 2005). There is no consensus about whether it represents a domain of Dinaric provenance (e.g., Pamić, 1997; Haas and Kovács, 2001), or it is related to the Meliata-Maliak ocean system (e.g., Goričan et al., 2005; Slovenec and Lugović, 2008; 2009; Slovenec et al., 2010). However, these basins belong to a back-arc basin belt that suffered the delayed subduction of the Paleotethyan lithosphere beneath the European continental margin (Stampfli and Borel, 2002; 2004). Late Anisian-Ladinian Ca-alkaline intermediate to acidic rocks and pyroclastics in association with continental blocks from the Mts. Žumberak and Mt. Ivanščica (Fig. 1A) which contain a Permian-Early to Middle Triassic sedimentary succession are interpreted as recording the magmatic activity on the active European continental margin (Goričan et al., 2005). According to this interpretation these magmatic rocks are related to Andean-type subduction and are not connected to the ophiolites.

It is not clear when the extensional tectonic activity caused by the upwelling of this OIB-type mantle plume into the ensialic back-arc lithosphere of the ROD really started. The related Illyrian (late Anisian) and Fassanian (early Ladinian) rifting in the ROD produced uncontaminated primitive and evolved alkali basalts, respectively (Fig. 10A). Apparent absence of crustal contamination in these alkali lavas suggests effusion in a highly evolved intracontinental rift basin. A Fassanian pelagic limestone interpillow matrix and high vesciculariy of the pillows (Halamić et al., 1998) indicate effusions above the CCD even in the terminal phase of intracontinental extension which still may coincide with subduction-related calc-alkaline magmatism in the Adria microplate. Similar Ladinian alkali basalts are reported from the Dinaride ophiolite zone (DOZ) by Vishnevskaya et al. (2009) and from Mts. Bükk in Hungary for a Middle Triassic analogue by Harangi et al. (1996). This fact may indicate large scale rifting of the continental lithosphere between the Adria microplate and the Tisia continental megablock of south Laurussia.

The formation of the first spreading ridge crust in the ROD is documented by enriched E-MORB-type basalt interlayered with late Fassanian to early Langobardian (early Ladinian) radiolarian cherts in the Mt. Kalnik. Formation of E-MORB extrusives indicate an initially slow-spreading ridge which allowed mixing between the uprising asthenosphere and the OIB-type mantle source; the onset of E-MORB-type crust generation continued to the Langobardian (late Ladinian), probably from a similar source successively depleted by previous E-MORB-type melt extraction resulting in depleted E-MORB-type crust (Fig 10B). Alkaline basalts produced by a low amount of partial melting may have formed simultaneously with E-MORB-type basalts at

this stage as oceanic islands or seamounts (Pe Piper, 1998). The ROD alkaline basalts are older, which precludes their interpretation as oceanic volcanic rocks related to this stage.

The transition from the proto-oceanic stage to evolved ocean spreading in the ROD is thought to be represented by the short-lived middle Carnian T-MORB-type basalts, which indicate derivation from a MORB-dominated mantle source enriched by components from residual material left after the previous partial melt evolution (Fig. 10C). In a modern ocean ridge analogue T-MORB basalts erupt simultaneously with N-MORB basalts (Reynolds et al., 1992, Haase, 2002; Geshi et al., 2007). The first true N-MORB-type crust in the ROD which is typical for the mature stage of an ocean (Fig 10C) is documented by late Carnian pillow basalts in frequent stratigraphic succession with radiolarian cherts in the Mt. Kalnik. At this stage only suboceanic N-MORB-type mantle contributes to magma genesis. Slight SSZ signature of these N-MORB-type basalts, expressed by a negative Ta-Nb anomaly, are inherited from the Middle Triassic subduction of Paleotethys (Fig. 10A). The next youngest ridge-related crust documented by the Pliensbachian and Bajocian (Early Jurassic) N-MORB-like gabbros (Pamić, 1997) still has SSZ signatures (our unpublished data) and is followed by Bajocian (Middle Jurassic) N-MORB basalts without subduction signature (Slovenec and Lugović, 2009). These facts promote Bajocian N-MOR basalts as the crust generated at the maximum evolved stage of spreading in the ROD and, moreover, suggest continuous oceanic ridge production for around 65 Ma, beginning in the early Ladinian (Fig. 10C).

The Mt. Medvednica N-MORB-type basalts dated to 165.4 Ma and 165.1 Ma (late Bathonian) with re-established subduction related influence (N-MORB with arc signatures of Shervais, 2001) signals the initiation of intraoceanic convergence in the ROD (Slovenec and Lugović, 2009). This stage is marked by subduction of an active oceanic ridge and formation of a metasomatized mantle wedge. The medium-Ti IAT basalt is dated to 164.7 Ma (latest Bathonian) and the low-Ti IAT varieties yield ages from 162.4 to 160.2 Ma (late Callovian to early Oxfordian.) consistent with the onset of partial melting and production of IAT-type basalts from increasingly depleted mantle (Slovenec and Lugović, 2009). The low-Ti IAT-type basalt from Mt. Ivanščica yielded an age of 154.7 Ma (Late Oxfordian) which is the

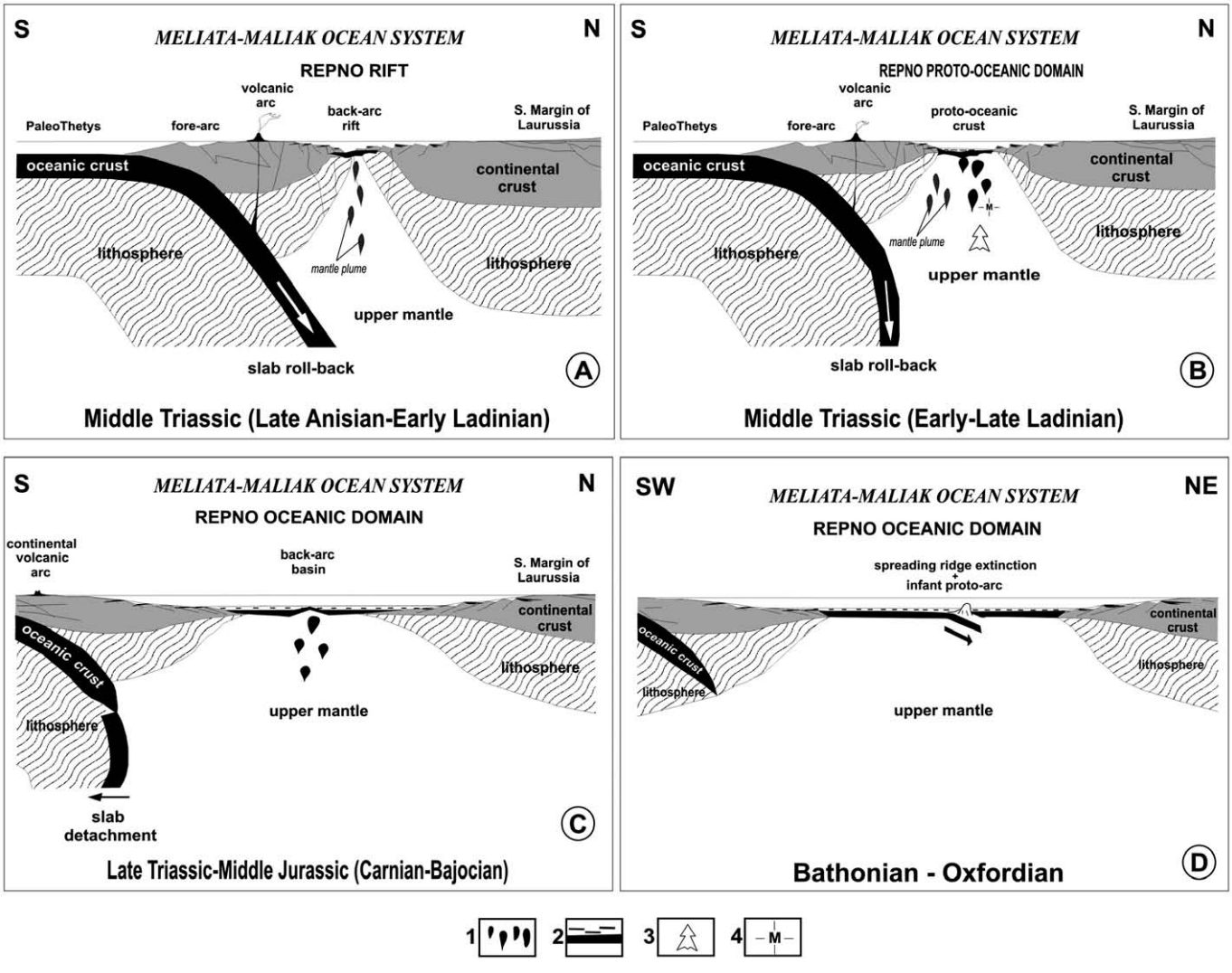

Fig. 10 - Schematic geodynamic evolutionary model for the ROD. (A) back-arc rifting, (B) initial drifting to spreading of proto-ocean, (C) long term active spreading and (D) subducting active spreading ridge and initiation of thrue subduction-related magmatic ativity. 1- mantle diapir, 2- oceanic crust topped by radiolarian cherts, 3- raising mantle diapir, 4- zone of partial melting.

youngest age recorded by magmatic rocks in the ROD. This rock shows the highest subduction components and reflects the most evolved composition produced in the protoarc extensional stage of the ROD.

The closure age of the ROD is inferred from the metamorphic rocks presumed to be ancient ROD crust. The lower greenschist facies metamorphic complex of Mt. Medvednica composed of IAT-type basalt protoliths (dated to 119±5 Ma by Belak et al., 1995), obducted onto the Adria continental margin (Lugović et al., 2006), and a metamorphic sole from the Mt. Kalnik which has BABB-type protoliths dated to 118±8 Ma (Ignjatić, 2007) suggest that the final closure took place during the Barremian-Aptian.

ACKNOWLEDGMENTS

This work is a contribution to the scientific projects on Mesozoic magmatic, mantle and pyroclastic rocks of northwestern Croatia (Grant no. 181-1951126-1141 to Da. S.) and on Tectonomagmatic correlation of fragmented oceanic lithosphere in the Dinarides (Grant no. 195-1951126-3205 to B. L.) carried out with the support of Croatian Ministry of Science, Education and Sport. We are very grateful to Josip Halamić for the use rock samples, as well as assistance in rocks sampling. Critical comments by Emilio Saccani and Riccardo Tribuzio helped to improve the final version of the manuscript.

REFERENCES

Agrawal S., Guevara M. and Verma S.P., 2008. Tectonic discrimination of basic and ultrabasic volcanic rocks through log-transformed ratios of immobile trace elements. Int. Geol. Rev., 50: 1057-1079.

Aldanmaz E., Yaliniz M.K., Güctekin A., Göncüoglu M.C., 2008. Geochemical characteristics of mafic lavas from the Neotethyan ophiolites in western Turkey: implications for heterogeneous source contribution during variable stages of ocean crust generation. Geol. Mag., 145: 37-54.

Babić Lj., Hochuli P.A. and Zupanič J., 2002. The Jurassic ophiolitic mélange in the NE Dinarides: dating, internal structure and geotectonic implications. Ecl. Geol. Helv., 95: 263-257.

Bébien J., Dimo-Lahitte A., Vergély P., Insergueix-Filippi D. and Dupeyrat L., 2000. Albanian ophiolites. I - Magmatic and metamorphic processes associated with the initiation of a subduction. Ofioliti, 25: 39-45.

Beccaluva L., Di Girolamo P., Macciotta G. and Morra V., 1983. Magma affinities and fractionation trends in ophiolites. Ofioliti, 8: 307-324.

Beccaluva L., Macciotta G., Piccardo G.B. and Zeda O., 1989. Clinopyroxene composition of ophiolite basalts as petrogenetic indicator. Chem. Geol., 77: 165-182.

Beccaluva L. and Serri G., 1988. Boninitic and low-Ti subduction-related lavas from intraoceanic arc-back-arc systems and low-Ti ophiolites: a reappraisal of their petrogenesis and original tectonic setting. Tectonophysics, 146: 291-315.

Belak M., Pamić J., Kolar-Jurkovšek T., Pecskay Z. and Karan D., 1995. Alpine low-grade regional metamorphic complex of Mt. Medvednica (northwest Croatia). In: I. Vlahović, I. Velić and M. Šparica (Eds.), Proceed., 1st Croat. Geol. Congr., Inst. Geol., Zagreb, p. 67-70 (in Croatian with English summary).

Bortolotti V., Carras N., Chiari M., Fazzuoli M., Marcucci M., Nirta G., Principi G. and Saccani E., 2009. The ophiolite-bearing mélange in the Early Tertiary Pindos flysch of Etolia (Central Greece). Ofioliti, 34: 83-94.

Bortolotti V., Chiari M., Kodra A., Marcucci M., Mustafa F., Principi G. and Saccani E., 2004. New evidence for Triassic MORB magmatism in the northern Mirdita Zone ophiolites (Albania). Ofioliti, 29: 243-246.

Bortolotti V., Marroni M., Pandolfi L., Principi G. and Saccani E., 2002. Interaction between mid-ocean ridge and subduction magmatism in Albanian ophiolites. J. Geol., 110: 561-576.

Bortolotti V. and Principi G., 2005. Tethyan ophiolites and Pangea break-up. Island Arc, 14: 442-470.

Cabanis B. and Leccole M., 1989. Le diagramme La/10-Y/15-Nb/8: un outil pour la discrimination des series volcaniques et la mise en evidence des processus de mélange et/ou de contamination crustale. C.R. Acad. Sci. Paris, Ser. II, 309: 2023-2029.

Cousens B.L., Allan J.F. and Gorton M.P., 1994. Subduction-modified pelagic sediments as the enriched component in back-arc basalts from the Japan Sea: Ocean Drilling Program Sites 797 and 794. Contrib. Mineral. Petrol., 117: 421-434.

Crawford A. and Keays R.R., 1987. Petrogenesis of Victorian Cambrian tholeiites and implcations for the origin of associated boninites. J. Petrol., 28: 1075-1109.

Dalrymple G.B. and Lanphere M.A., 1969. Potassium-argon dating: principles, techniques and applications to geochronology. Freeman W.H. San Francisco, 67 pp.

Dilek Y., Furnes H. and Shallo M., 2007. Suprasubduction zone ophiolite formation along the periphery of Mesozoic Gondwana. Gondwana Res., 11: 453-475.

Ewart A., Bryan W.B., Chappell B.W. and Rudnick R.L., 1994. 24. Regional geochemistry of the Lau-Tonga arc and back arc system. In: J. Hawkins, L. Parson and J. Allan (Eds.), Proceed. O.D.P. Sci. Res., 135: 385-425.

Ewart A., Collerson K.D., Regelous M., Wendt J.I. and Niu Y., 1998. Geochemical evolution within the Tonga-Kermadec-Lau arc-back-arc system: the role of varying mantle wedge composition in space and time. J. Petrol., 39: 331-368.

Festa A., Pini G.A., Dilek Y. and Codegone J., 2010. Mélanges and mélange-forming processes: a historical overview and new concepts. Int. Geol. Rev., 52: 1040-1105.

Fitton J.G., 2007. The OIB paradox. In: G.R. Foulger and D.M. Jurdy (Eds.), Plates, plume and planetary processes. Geol. Soc. Am. Spec. Paper, 430: 387-412.

Geshi N., Umino S., Kumagai H., Sinton J.M., White S.M., Kisimoto K. and Hilde T.W., 2007. Dicrete plumbing systems and heterogeneous magma sources of a 24 km^3 off-axis lava field on the western flank of East Pacific Rise, 14°S. Earth Planet. Sci. Lett., 258: 61-72.

Golub Lj. and Vragović M., 1960. Sodium diabase and spilite near Gotalovec in the province of Hrvatsko Zagorje. JAZU, Acta Geol., 1: 83-93 (in Croatian with English summary).

Golub Lj. and Šiftar D., 1965. Eruptive rocks from the southern slopes of Mt. Ivanščica (Hrvatsko Zagorje-Yugoslavia). Acta Geol., 4: 341-347 (in Croatian with English summary).

Goričan Š., Halamić J., Grgasović T. and Kolar-Jurkovšek T., 2005. Stratigraphic evolution of Triassic arc-backarc system in northwestern Croatia. Bull. Soc. Géol. France, 176: 3-22.

Gökten E. and Floyd P.A., 2007. Stratigraphy and geochemistry of pillow basalts within the ophiolitic mélange of the Izmir-Ankara-Erzincan suture zone: implications for the geotectonic character of the northern branch of Neotethys. Int. J. Earth Sci., 96: 725-741.

Göncüoglu M.C., Sayit K. and Tekin U.K., 2010. Oceanization of the northern Neotethys: geochemical evidence from ophiolitic melange basalts within the İzmir-Ankara suture belt, NW Turkey. Lithos, 116: 175-187.

Gribble R.F., Stern R.J., Newman S., Bloomer S.H. and O`Hearn T., 1998. Chemical and isotopic composition of lavas from the Northern Mariana Trough: implications for magmagenesis in back-arc basins. J. Petrol., 39: 125-154.

Haas J. and Kovács S., 2001. The Dinaridic-Alpine connection - as seen from Hungary. Acta Geol. Hungar., 44: 345-362.

Haas J., Mioč P., Pamić J., Tomljenović B., Árkai P., Bérczi-Makk A., Koroknai B., Kovács S. and R.-Felgenhauer E., 2000. Complex structural pattern of the Alpine-Dinaridic Pannonian triple junction. Int. J. Earth Sci., 89: 377-389.

Haase K.M., 2002. Geochemical constraints on magma sources

and mixing processes in Easter Microplate MORB (SE Pacific): a case study of plume-ridge interaction. Chem. Geol., 182: 335-355.

Haase K.M. and Devey C.W., 1996. Geochemistry of lavas from the Ahu and Tupa volcanic felds, Easter Hotspot, southeast Pacific: Implications for magma genesis near a spreading axis. Earth Planet. Sci. Lett., 137: 129-143.

Halamić J., 1998. Lithostratigraphy of Jurassic and Cretaceous sediments with ophiolites from the Mts. Medvednica, Kalnik and Ivanščica. PhD Thesis, University of Zagreb, Zagreb, 188 pp (in Croatian with English summary).

Halamić J. and Goričan Š., 1995. Triassic radiolarites from Mts. Kalnik and Medvednica (Northwestern Croatia). Geol. Croatica, 48: 129-146.

Halamić J., Slovenec Da. and Kolar-Jurkovšek T., 1998. Triassic pelagic limestones in pillow lavas in the Orešje quarry near Gornja Bistra, Medvednica Mt. (Northwest Croatia). Geol. Croatica, 51: 33-45.

Harangi Sz., Szabó Cs., Józsa S., Szoldán Zs., Árva-Sós E., Balla M. and Kubovics I., 1996. Mesozoic igneous suites in Hungary: implications for genesis and tectonic setting in the northwestern part of Tethys. Int. Geol. Rev., 38: 336-360.

Hart S.R., Wolde G.C., Walter R.C. and Mertzman S.A., 1989. Basaltic volcanism in Ethiopia: constraints on continental rifting and mantle intractions. J. Geoph. Res., 94: 7731-7748.

Hoeck V., Koller F., Meisel T., Onuzi K. and Kneringer E., 2002. The Jurassic South Albanian ophiolites: MORB- vs. SSZ-type ophiolites. Lithos, 65: 143-164.

Ignjatić S., 2007. Upper Cretaceous amphibolites from lherzolite metamorphic sole (Kalnik Mt., Croatia). Grad. Thesis, Univ. Zagreb, Zagreb, 61 pp (in Croatian with English summary).

Ikeda Y. and Yuasa M., 1989. Volcanism in nascent back-arc basin behind the Shichito Ridge and adjecent areas in the Izu-Ogaswara arc, northwest Pacific. Contrib. Mineral. Petrol., 101: 377-393.

Jahn B., 1986. Mid-ocean ridge or marginal basin origin of the East Taiwan Ophiolite: chemical and isotopic evidence. Contrib. Mineral. Petrol., 92: 194-206.

Koglin N., Kostopoulos D. and Reischmann T., 2009. The Lesvos mafic-ultramafic complex, Greece: ophiolite or incipient rift? Lithos, 108: 243-261.

Leat P.T., Livermore R.A., Millar I.L. and Pearce J.A., 2000. Magma supplay in back-arc spreding centre segment E2, East Scotia Ridge. J. Petrol., 41: 845-866.

Leterrier J., Maury R. C., Thonon P., Girrard D. and Marchal M., 1982. Clinopyroxene composition as a method of identification of the magmatic affinities of paleovolcanic series. Earth Planet. Sci. Lett., 59: 139-154.

Lugović B., Altherr R., Raczek I., Hofmann A.W. and Majer V., 1991. Geochemistry of peridotites and mafic igneous rocks from the Central Dinaric Ophiolite Belt, Yugoslavia. Contrib. Mineral. Petrol., 106: 201-216.

Lugović B., Šegvić B. and Altherr R., 2006. Petrology and tectonic significance of greenschists from the Medvednica Mts. (Sava Unit, NW Croatia). Ofioliti, 31: 39-50.

Lugović B., Slovenec D., Halamić J. and Altherr R., 2007. Petrology, geochemistry and geotectonic affinity of the Mesozoic ultramafic rocks from the southwesternmost Mid-Transdanubian Zone in Croatia. Geol. Carpath., 58: 511-530.

McKenzie D. and O'Nions R.K. 1991. Partial melt distributions from inversion of rare earth element concentrations. J. Petrol., 32: 1021-1091.

Monjoie P., Lapierre H., Tashko A., Mascle G.H., Dechamp A., Muceku B. and Brunet P., 2008. Nature and origin of the Triassic volcanism in Albania and Othrys: a key to understanding the Neotethys opening? Bull. Soc. Géol. France, 179: 411-425.

Morimoto N., 1988. Nomenclature of pyroxenes. Schweiz. Mineral. Petrol. Mitt., 68: 95-111.

Münker C., 2000. The isotope and trace element budget of the Cambrian Devil River arc system, New Zealand: identification of four source components. J. Petrol., 41: 759-788.

Nisbet E.G. and Pearce J.A., 1977. Clinopyroxene composition in mafic lavas from different tectonic settings. Contrib. Mineral. Petrol., 63: 149-160.

Ogg J.G., 2004. The Jurassic period. In: F.M. Gradstein, J.G. Ogg and A.G. Smith (Eds.), A Geologic Time Scale, Cambridge University Press, p. 307-343.

Okamura S., Arculus R.J. and Martynov Y.A., 2005. Cenozoic magmatism of the North-Eastern Eurasian Margin: The role of lithosphere versus astenosphere. J. Petrol., 46: 221-253.

Palinkaš L.A., Bermanec V., Borojević-Šoštarić S., Kolar-Jurkovšek T., Strmić-Palinkaš S., Molnar F. and Kniewald G., 2008. Volcanic facies analysis of a subaqueous basalt lava-flow complex at Hruškovec, NW Croatia - evidence of advanced rifting in the Tethyan domain. J. Volcanol. Geotherm. Res., 178: 644-656.

Pamić J., 1997. The northwesternmost outcrops of the Dinaridic ophiolites: a case study of the Mt. Kalnik (North Croatia). Acta Geol. Hungar., 40: 37-56.

Pamić J., 2000. The Periadriatic-Sava-Vardar Suture Zone. In: I. Vlahović and R. Biondić (Eds.), Proceed. 2nd Croat. Geol. Congr., Inst. Geol., Zagreb, p. 333-337.

Pamić J., 2002. The Sava-Vardar Zone of the Dinarides and Hellenides versus the Vardar Ocean. Ecl. Geol. Helv., 95: 99-113.

Pamić J. and Tomljenović B., 1998. Basic geological data on the Croatian part of the Mid-Transdanubian Zone as exemplified by Mt. Medvednica located along the Zagreb-Zemplen Fault Zone. Acta Geol. Hungar., 41: 389-400.

Pe-Piper G., 1998. The nature of Triassic extension-related magmatism in Greece: evidence from Nd and Pb isotope geochemistry. Geol. Mag., 135: 331-348.

Pearce J.A., 1983. Role of the sub-continental lithosphere in magma genesis at active continental margins. In: C.J. Hawkesworth and M.J. Norry (Eds.), Continental basalts and mantle xenoliths. Shiva, Nantwich, p. 230-249.

Pearce J.A., Baker P.E., Harvey P.K. and Luff I.W., 1995. Geochemical evidence for subduction fluxes, mantle melting for fractional crystalization beneath the South Sandwich island arc. J. Petrol., 36: 1073-1109.

Pearce J.A., Lippard S.J. and Roberts S., 1984. Characteristics and tectonic significance of supra-subduction zone ophiolites. In: B.P. Kokelaar and M.F. Howells (Eds.), Marginal basin geology. Geol. Soc. London Spec. Publ., 16: 17-94.

Peate D.W., Pearce J.A., Hawkesworth C.J., Colley H., Edwards M.H. and Hirose K., 1997. Geochemical variations in Vanuatu arc lavas: the role of subducted material and a variable mantle wedge composition. J. Petrol., 38: 1331-1358.

Poljak J., 1942. Ein beitrag zur Geologie des Kalnik-Gebirges. Vjestnik Hrv. Drž. Geol. Zav. i Geol. Muz., 1: 53-92. (in Croatian with German summary).

Pouchou J.L. and Pichoir F., 1984. A new model for quantitative analyses. I. Application to the analysis of homogeneous samples. La Rech. Aérosp., 3: 13-38.

Pouchou J.L. and Pichoir F., 1985. "PAP" (ϕ-ϱ-Z) correction procedure for improved quantitative microanalysis. In: J.T. Armstrong (Ed.), Microbeam analysis. San Francisco Press, p. 104-106.

Reynolds J.R., Langmuir C.H., Bender J.F., Kastens K.A. and Ryan W.B.F., 1992. Spatial and temporal variability in the geochemistry of basalts from the East Pacific Rise. Nature, 359: 493-499.

Robertson A.H.F., 2002. Overview of the genesis and emplacement of Mesozoic ophiolites in the Eastern Mediterranean region. Lithos, 65: 1-68.

Robertson A.H.F. and Shallo M., 2000. Mesozoic-Tertiary tectonic evolution of Albania in its regional Eastern Mediterranean context. Tectonophysics, 316: 197-214.

Rojay B., Yaliniz K.M. and Altiner D., 2001. Tectonic implications of some cretaceous pillow basalts from the North Anatolian ophiolitic mélange (Central Anatolia-Turkey) to the evolution of Neotethys. Turkish J. Earth Sci., 10: 93-102.

Saccani E., Beccaluva L., Photiades A. and Zeda O., 2010. Petro-

genesis and tectono- magmatic significance of basalts and mantle peridotites from the Albanian-Greek ophiolites and subophiolitic mélanges. New constraints for the Triassic-Jurassic evolution of the Neo-Tethys in the Dinaride sector. Lithos, doi:10.1016/j.lithos.2010.10.009.

Saccani E., Padoa E. and Photiades A., 2003. Triassic mid-ocean ridge basalts from the Argolis Peninsula (Greece): new constraints for the early oceanization phases of the Neo-Tethyan Pindos basin. In: Y.Dilek and P.T. Robinson (Eds.), Ophiolites in earth history, Geol. Soc. London Spec. Publ., 218: 109-127.

Saccani E. and Photiades A., 2005. Petrogenesis and tectonomagmatic significance of volcanic and subvolcanic rocks in the Albanide-Hellenide ophiolitic mélanges. Island Arc, 14: 494-516.

Saunders A.D. and Tarney J., 1979. The geochemistry of basalts from a back-arc spreading center in the East Scotia Sea. Geochim. Cosmochim. Acta, 43: 555-572.

Schmid S.M., Bernoulli D., Fügenschuh B., Matenco L., Scheffer S., Schuster R., Tischler M. and Ustaszewski K., 2008. The Alpine-Carpathian-Dinaridic orogenic system: correlation and evolution of tectonic units. Swiss J. Geosci., 101: 139-183.

Serri S., 1981. The petrochemistry of ophiolitic gabbro-complexes: a key for classification of ophiolites to low-Ti and high-Ti types. Earth Planet. Sci. Lett., 52: 203-212.

Shervais J.W., 1982. Ti-V plots and petrogenesis of modern and ophiolitic lavas. Earth Planet. Sci. Lett., 59: 101-118.

Shervais J.W., 2001. Birth, dead, and resurrection: the life cycle of supra-subduction zone ophiolites. Geochemistry, Geophysics, Geosciences, v. 2 [2000GC000080].

Shiffman P. and Lofgren G.E., 1982. Dinamic crystallization studies on the Grande Ronde pillow basalts, Central Washington. J. Geol., 90: 49-78.

Slovenec Da. and Lugović B., 2008. Amphibole gabbroic rocks from the Mt. Medvednica ophiolite mélange (NW Croatia): geochemistry and tectonic setting. Geol. Carpath., 59: 277-293.

Slovenec D. and Lugović B., 2009. Geochemistry and tectonomagmatic affinity of extrusive and dyke rocks from the ophiolite mélange in the SW Zagorje-Mid-Transdanubian Zone (Mt. Medvednica, Croatia). Ofioliti, 34: 63-80.

Slovenec Da., Lugović B. and Vlahović I., 2010. Geochemistry, petrology and tectonomagmatic significance of basaltic rocks from the ophiolite mélange at the NW External-Internal Dinarides junction (Croatia). Geol. Carpath., 61: 273-294.

Smith A.G., Hynes A.J., Menzies A.J., Nisbet E.G., Price I., Welland M.J.P. and Ferrière J., 1975. The stratigraphy of the Othris Mountains, eastern central Greece. Ecl. Geol. Helv., 68: 463-481.

Spath A., Le Roex A.P. and Opivo-Akech N., 2001. Plume lithosphere interaction and the origin of continental rift-related alkaline volcanism - the Chyulu Hills volcanic Province, Soutern Kenya. J. Petrol., 42: 765-787.

Stampfli G.M. and Borel G.D., 2002. A plate tectonic model for the Paleozoic and Mesozoic constrained by dinamic plate boundaries and restored synthetic ocean isochrons. Earth Planet. Sci. Lett., 196: 17-33.

Stampfli G.M. and Borel G.D. 2004. The TRANSMED transects in space and time: Constraints on the paleotectonic evolution of the Mediterranean domain. In: Cavazza W. Roure F., Spakman W., Stampfli G.M. and Ziegler P.A. (Eds.). The TRANSMED Atlas: the Mediterranean Region from crust to mantle. Springer Verlag, p 53-80.

Stern C., 2004. Subduction initiation: spontaneous and induced. Earth Planet. Sci. Lett., 226: 275-292.

Sun S.S. and McDonough W.F., 1989. Chemical and isotopic systematics of oceanic basalts: implications for mantle composition and processes. In: A.D. Saunders and M.J. Norry (Eds.), Magmatism in ocean basins. Geol. Soc. London Spec. Publ., 42: 313-345.

Šimunić A., Pikija M., Hećimović I. and Šimunić A., 1981. Basic geological map 1:100.000. Sheet Varaždin, explanatory notes. Inst. Geol. Istraž. Zagreb - Sav. Geol. Zavod, Beograd, 1-81 (in Croatian with English summary).

Šimunić A., Pikija M. and Hećimović I., 1982. Basic geological map 1:100.000. Sheet Varaždin, Inst. Geol. Istraž. Zagreb - Sav. Geol. Zavod, Beograd.

Tari V. and Pamić J., 1998. Geodynamic evolution of the Northern Dinarides and the southern parts of the Pannonian Basin. Tectonophysics, 297: 296-281.

Taylor S.R. and McLennan S.M., 1985. The continental crust: its composition and evolution. Blackwell, Oxford, 312 pp.

Tomljenović B., Csontos L., Márton E. and Márton P., 2008. Tectonic evolution of the northwestern Internal Dinarides as constrained by structures and rotation of Medvednica Mountains, North Croatia. Geol. Soc. London Spec. Publ., 298: 145-167.

Tracy R.J. and Robinson P., 1977. Zoned titanium augite in alkali olivine basalt from Tahiti and the nature of titanium substitutions in augite. Am. Mineral., 62: 634-645.

Trubelja F., Marching V., Burgath K.-P. and Vujović Ž., 1995. Origin of the Jurassic Tethyan ophiolites in Bosnia: a geochemical approach to tectonic setting. Geol. Croath., 48: 49-66.

Vishnevskaya V.S., Djerić N and Zakariadze G.S., 2009. New data on Mesozoic radiolaria of Serbia and Bosnia, and implications for the age and evolution of oceanic volcanic rocks in the Central and Northern Balkans. Lithos, 108: 72-105.

Vrkljan M., 1988. Eruptive rocks from Paka brook (Mt. Kalnik, NW Croatia). Geol. Vjesnik., 41: 133-144 (in Croatian with English summary).

Vrkljan M., 1989. Eruptive rocks from Mt. Kalnik. PhD Thesis, Univ. Zagreb, 1-94 (in Croatian with English summary).

Vrkljan M.,1992. Spilite from Kamešnica, Mt. Kalnik, NW Croatia. Geol. Croath., 45: 53-61.

Vrkljan M., 1994. Petrographic characteristics of extrusive rocks from Hruškovec, Mt. Kalnik, NW Croatia. Geol. Croath., 47: 181-191.

Vrkljan M. and Garašić V., 2004. Different geochemical signatures developed in some basic magmatic rocks of Mt. Kalnik (North Croatia). Rudar. Geol. Naftni Zbornik, 16: 65-73.

Vrkljan M. and Vragović M., 1991. Spilites from the upper streams of creeks Glogovnica and Rakov potok (Mt. Kalnik, NW Croatia). Geol. Vjesnik, 44: 181-193.

Weaver D.S., Saunders A.D., Pankhurst R.J. and Tarney J., 1979. A geochemical study of magmatism associated with the initial stages of back-arc spreading. Contrib. Mineral. Petrol., 68: 151-169.

Weaver B.L. and Tarney J., 1984. Empirical approach to estimating the composition of the continental crust. Nature, 310: 585-588.

Wilson M., 1989. Igneous petrogenesis. Unwin Hyman Ltd., London, 465 pp.

Winchester J.A. and Floyd P.A.,1977. Geochemical discrimination of different magma series and their differentiation products using immobile elements. Chem. Geol., 20: 325-343.

Wood D.A., 1980. The application of a Th-Hf-Ta diagram to problems of tectonomagmatic classification and establishing the nature of crustal contamination of basaltic lavas of the British Tertiary volcanic province. Earth Planet. Sci. Lett., 50: 11-30.

Zindler A. and Hart S.R., 1986. Chemical geodynamics. Ann. Rev. Earth Planet. Sci., 14: 439-571.

Received, May 12, 2009
Accepted, March 16, 2011